

Pre-training Differentially Private Models with Limited Public Data

Zhiqi Bu^{*1}, Xinwei Zhang^{*†2}, Mingyi Hong^{‡2}, Sheng Zha¹, and George Karypis¹

¹Amazon Web Services AI

²University of Minnesota

Abstract

The superior performance of large foundation models relies on the use of massive amounts of high-quality data, which often contain sensitive, private and copyrighted material that requires formal protection. While differential privacy (DP) is a prominent method to gauge the degree of security provided to the models, its application is commonly limited to the model fine-tuning stage, due to the performance degradation when applying DP during the pre-training stage. Consequently, DP is yet not capable of protecting a substantial portion of the data used during the initial pre-training process.

In this work, we first provide a theoretical understanding of the efficacy of DP training by analyzing the per-iteration loss improvement. We make a key observation that DP optimizers' performance degradation can be significantly mitigated by the use of limited public data, which leads to a novel DP continual pre-training strategy. Empirically, using only 10% of public data, our strategy can achieve DP accuracy of 41.5% on ImageNet-21k (with $\epsilon = 8$), as well as non-DP accuracy of 55.7% and 60.0% on downstream tasks Places365 and iNaturalist-2021, respectively, on par with state-of-the-art standard pre-training and substantially outperforming existing DP pre-trained models.

1 Introduction

Pre-trained large models have been the backbone of computer vision and natural language processing. Finetuning or zero/few-shots learning (including in-context learning) based on these models can achieve superior performance. In particular, differentially private (DP) fine-tuning, such as full-parameter training, LoRA, Adapter, BiTFiT, and linear probing [88, 48, 11, 12, 57], has shown to be almost as accurate as the standard non-DP fine-tuning on GPT [67, 6], ViT [26], and ResNet [38] models, while protecting the privacy of fine-tuning data privacy. To be more specific, DP language models (GPT2/BERT/RNN) and vision models are highly effective in defending against canary insertion attacks [65, 39, 41] and membership inference attacks [19, 68, 31, 15]; DP fine-tuned GPT2 also reduces the personally identifiable information leakage by 5 – 10 times compared with its Non-DP counterpart[52].

These DP fine-tuned models all follow a two-stage training procedure, in which the first stage trains a pre-trained model on large public datasets (without privacy protection), and the second stage fine-tunes on relatively small private datasets. However, a growing concern has been raised against the pre-training on the vast amount of web-collected data [17, 16, 77, 40, 61, 66]. The pre-trained models could memorize and re-generate the sensitive information in the training data, which include copyright content in books and codes, images of faces and nudity, and other personally identifiable information such as address and phone numbers, even if the data have been pre-processed by some content filters. While it is common to use close-source or proprietary datasets instead and not to release the models trained on them, this approach renders the models not reproducible and still violates data privacy in a more implicit way.

Consequently, because of the uncertainty in seemingly safe-to-use public datasets, it is important to apply DP to the pre-training phase, which is computationally feasible, since DP optimization can be as efficient as the standard Non-DP training [13, 37]. However, DP optimization without any public data suffers from slow convergence, and suboptimal performance: even on CIFAR10, the accuracy drops from $> 95\%$ to $< 70\%$ at $\epsilon = 8$ [62]; on GPT2, the non-DP BLEU score degrades from 65.73 (quality often better than human) to 15.457 (hard to get the gist) at

^{*}Equal contribution. Email: zhiqibu@amazon.com

[†]Work done during an internship at Amazon.

[‡]MH holds concurrent appointments as an Amazon Scholar and as a faculty at University of Minnesota. This paper describes his work performed at Amazon.

$\epsilon = 3$ [48]. In short, pre-training and fine-tuning differ significantly in the amount of data and computation resources used, as well as in optimization setups. We summarize the difference between DP pre-training and DP fine-tuning in Table 1.

Table 1: Comparing DP pre-training and DP fine-tuning.

	pre-training	fine-tuning
Dataset size	large	small
Public data size used	small	large
Training iterations	large	small
Trainable parameters	100%	0.1-100%

1.1 Contributions

Our main contributions are listed below.

- (1) We provide a new perspective of analyzing the loss improvement in DP training with different optimizers. Specifically, we propose a Hessian-based framework to analyze the per-iteration improvement on the generalization loss and the effects of per-sample gradient clipping, noising, and hyperparameter choices (e.g., batch size, learning rate).
- (2) Based on the framework, we can analyze the effect that DP mechanisms, especially the DP noise, have on pre-training and fine-tuning stages, leading to some theoretical justifications about why pre-training is more vulnerable to DP noise; see Figure 1 for some empirical comparisons, and Section 3 for some in-depth discussion.
- (3) Our analysis suggests that the deceleration due to DP mechanisms can be mitigated by using a certain amount of public data. We then propose a DP continual pre-training strategy that continues the pre-training privately from a non-DP initialization. Our strategy is easily implementable, automatic, and effective, which obtains accuracy on upstream and downstream tasks that is on par with its non-DP variants, while significantly outperforming state-of-the-art DP pretraining algorithms (see Figure 2). We will open-source our DP pre-trained vision models.

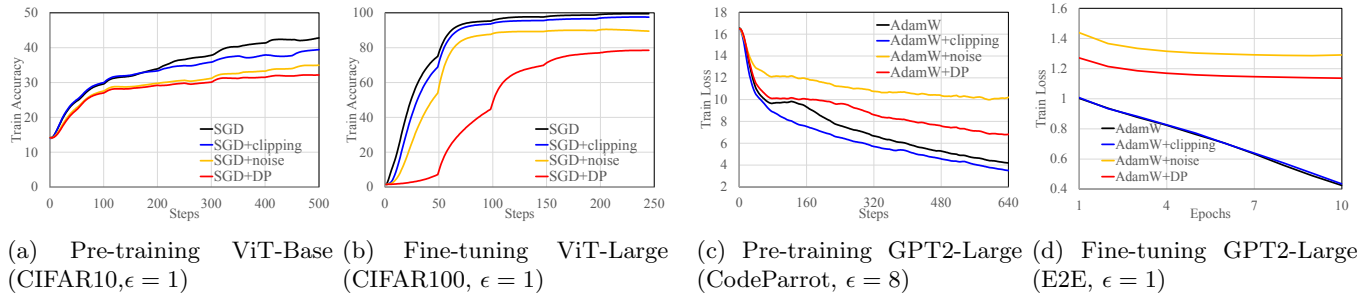


Figure 1: Comparison among the convergence of standard SGD, clipped SGD, noisy SGD, and DP-SGD in different tasks and training stages.

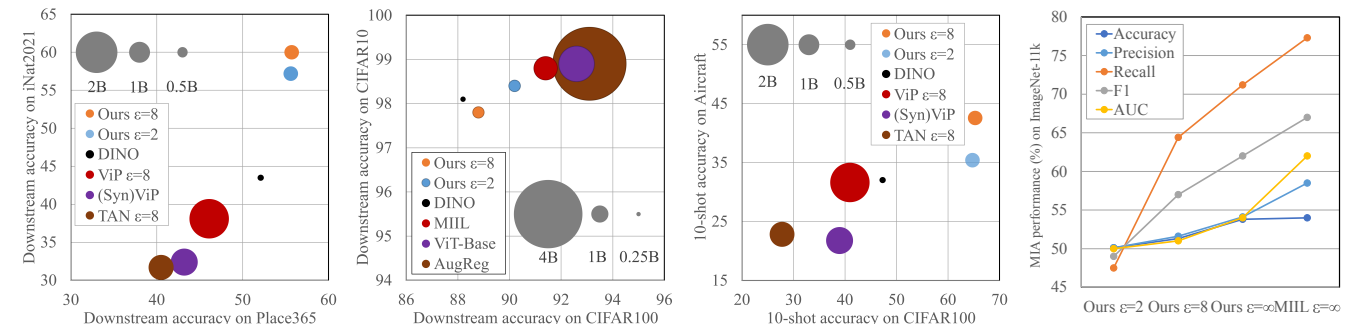


Figure 2: Summary of results in Section 5. First three figures compare the downstream and few-shot performance and the data efficiency (circle’s radius proportional to pre-training data size) of the DP pre-trained vision models; the last figure shows the performance of DP pre-trained models defending against privacy attacks (lower is more private).

1.2 Related works

This work is closely related to other works in DP convergence analysis, DP fine-tuning of large models, the continual training and the Hessian-based analysis. We refer to Appendix C for an extended discussion.

1.3 Notions & settings

We denote the mini-batch size as B with index set \mathcal{B} , dataset size as n , number of training iterations as T , iteration index as $t \leq T$, learning rate as η , model parameters as $\mathbf{w} \in \mathbb{R}^d$, and training samples as x . We use $\{\text{k, M, B}\}$ for $\{\text{thousand, million, billion}\}$.

We study DP optimization under fixed budgets for computation (with a fixed number of samples), privacy (with a fixed DP guarantee), and limited availability of public data.

1.4 Computation budget

We consider a fixed computation budget, so that the training ends when a fixed number of samples $S := BT$ have been processed. As B increases, the number of iterations T decreases linearly, while the per-iteration training time increases almost linearly. This is because foundation models are generally trained with large batch size, which requires the use of distributed learning and gradient accumulation¹. For example, Vision Transformers (ViT, [26, 73]) is trained with $B = 4\text{k}$, GPT-3 [6] and LLaMA [75] with $B \approx 2\text{k}$, DP-ResNet/ViT with $B = 4\text{k}$ in [23] and $B = 1\text{M}$ in [57], DP-RoBERTa with $B = 2\text{k}$ in [88], and DP-GPT2 with $B = 1\text{k}$ in [48].

As a consequence, the batch size B has nearly zero influence on the total training time, focusing its effect only on the convergence speed.

1.5 Privacy budget

Definition 1.1 ([28, 25]). A randomized algorithm \mathcal{M} is (ϵ, δ) -DP if, for any two neighboring datasets $\mathcal{S}, \mathcal{S}'$ that differ by one sample and for any event \mathcal{E} ,

$$\mathbb{P}[\mathcal{M}(\mathcal{S}) \in \mathcal{E}] \leq e^\epsilon \mathbb{P}[\mathcal{M}(\mathcal{S}') \in \mathcal{E}] + \delta, \text{ where } \delta < 1/n.$$

We consider a fixed privacy budget (ϵ, δ) , to be realized through the DP optimizers in (2). Essentially, a noise $\sigma\mathcal{N}(0, \mathbf{I})$ is injected to the gradient at each iteration, whereas the noise magnitude $\sigma(B)$ is determined by privacy accountants such as RDP (default) [58], PRV [33] and GDP [25, 7] (see Figure 3).

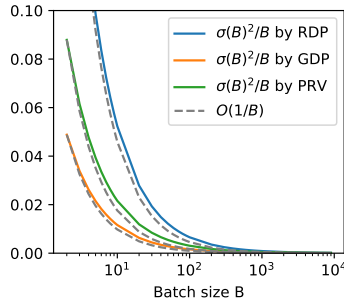


Figure 3: Noise levels by privacy accountants.

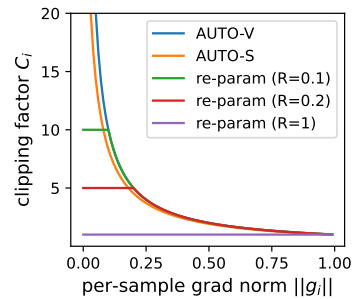


Figure 4: Per-sample gradient clipping in (3).

2 Understanding DP training through the lens of Hessian

In this section, we derive the impact of different components in DP training (including the per-sample clipping, the noising, and hyper-parameter choices), by characterizing the per-iteration per-sample loss improvement through the lens of Hessian.

¹The mini-batch of size B (a.k.a. the logical batch size) is divided into B/b micro-batches, where the micro-batch size is $b \ll B$ (a.k.a. the physical or per-GPU batch size, which determines the training speed and memory cost). When b is fixed subject to GPU memory, the per-iteration training time is proportional to the number of micro-batches and thus to B .

To begin with, we consider the task of optimizing the generalization loss (equivalently the expected risk) for any differentiable loss function, e.g. the cross entropy or adversarial loss [32]:

$$\min_{\mathbf{w} \in \mathbb{R}^d} L(\mathbf{w}) = \mathbb{E}_x[L(\mathbf{w}, x)]. \quad (1)$$

We denote the per-sample gradient $\mathbf{g}_i(\mathbf{w}) := \frac{\partial L(\mathbf{w}, x_i)}{\partial \mathbf{w}} \in \mathbb{R}^d$, the oracle gradient $\mathbf{G}(\mathbf{w}) := \frac{\partial \mathbb{E}_x[L(\mathbf{w}, x)]}{\partial \mathbf{w}} \in \mathbb{R}^d$, and the oracle Hessian matrix $\mathbf{H}(\mathbf{w}) := \frac{\partial^2 \mathbb{E}_x[L(\mathbf{w}, x)]}{\partial \mathbf{w}^2} \in \mathbb{R}^{d \times d}$. In Assumption 2.1, samples follow identically and independently (i.i.d.) from some data distribution, with no restriction on the covariance structure $\Sigma(\mathbf{w})$.

Assumption 2.1. Per-sample gradients $\mathbf{g}_i(\mathbf{w})$ are i.i.d with

$$\mathbb{E}[\mathbf{g}_i(\mathbf{w})] = \mathbf{G}(\mathbf{w}), \quad \text{Cov}(\mathbf{g}_i(\mathbf{w})) = \Sigma(\mathbf{w}).$$

To simplify the notation, we drop the dependence on \mathbf{w} .

Consider the general DP optimizers, including SGD and Adam [45], which update the parameters with the privatized gradient,

$$\mathbf{g} = \frac{\sum_{i \in \mathcal{B}} C_i \mathbf{g}_i + \sigma \mathcal{N}(0, \mathbf{I}_d)}{B} \approx \frac{c \sum_{i \in \mathcal{B}} \mathbf{g}_i + \sigma \mathcal{N}(0, \mathbf{I}_d)}{B}. \quad (2)$$

Here $C_i := C(\|\mathbf{g}_i\|; R)$ is the per-sample clipping factor that restricts the sensitivity of $\sum_i C_i \mathbf{g}_i$ to some constant R , i.e. $\|C_i \mathbf{g}_i\| \leq R$. We set $\|C_i \mathbf{g}_i\| \leq 1$ (thus omitting R throughout the paper) following the re-parameterized gradient clipping [23] and the automatic (AUTO) clipping [11], whose C_i 's are listed below:

$$C_{i,\text{re-param}} = \min \left\{ \frac{1}{\|\mathbf{g}_i\|}, \frac{1}{R} \right\} \quad \text{or} \quad C_{i,\text{AUTO}} = \frac{1}{\|\mathbf{g}_i\|}. \quad (3)$$

Figure 4 illustrates the values of C_i under different clipping functions. Note that in (2), we employ a crucial approximation $c \approx \mathbb{E}[C_i]$ so as to unify the formula of DP and non-DP SGD in Remark 2.2. This approximation only holds when the directions of vectors $\sum_i C_i \mathbf{g}_i$ and $\sum_i \mathbf{g}_i$ are very close, i.e., there is little *per-sample clipping bias*. Such approximation is validated in Figure 1, where we observe from the ‘SGD’ and ‘SGD+clipping’ curves that the convergence (without noising) is not much influenced by the bias of per-sample gradient clipping.

Remark 2.2. Setting $c = 1$ and $\sigma = 0$, the gradient (2) reduces to the standard minibatch gradient. Hence, the difference between SGD and DP-SGD is characterized by (σ, c) .

Per-iteration improvement of DP-SGD: Next, we characterize and analyze the per-iteration improvement of DP-SGD through the lens of Hessian, under different choices of hyperparameters and clipping functions:

$$\mathbf{w}_{t+1} = \mathbf{w}_t - \eta \mathbf{g}_t. \quad (4)$$

The extension of the analysis to more general optimizers (e.g., DP-Adam) is given in Section 3.4. We are interested in minimizing the second-order Taylor expansion of $L(\mathbf{w} - \eta \mathbf{g})$, which is sufficiently accurate since parameter updates are often quite small [56]. The loss improvement in one iteration can be approximated as:

$$L(\mathbf{w}) - L(\mathbf{w} - \eta \mathbf{g}) \approx \eta \mathbf{G}^\top \mathbf{g} - \frac{\eta^2}{2} \mathbf{g}^\top \mathbf{H} \mathbf{g}.$$

Taking the expectation, we obtain the expected per-iteration loss improvement (derived in Appendix A.1):

$$\Delta L := \eta \mathbf{G}^\top \mathbb{E}[\mathbf{g}] - \frac{\eta^2}{2} (\text{tr}(\mathbf{H} \text{Cov}(\mathbf{g})) + \mathbb{E}[\mathbf{g}]^\top \mathbf{H} \mathbb{E}[\mathbf{g}]). \quad (5)$$

By applying Assumption 2.1, we have

$$\mathbb{E}[\mathbf{g}] = c \mathbf{G}, \quad \text{Cov}(\mathbf{g}) = c^2 \Sigma / B + \sigma^2 / B^2.$$

Substitute to (5), we obtain a quadratic function of η :

$$\Delta L_{\text{priv}}(\eta, B) := \eta c \mathbf{G}^\top \mathbf{G} - \frac{\eta^2}{2} \left(c^2 \mathbf{G}^\top \mathbf{H} \mathbf{G} + \frac{c^2 \text{tr}(\mathbf{H} \Sigma)}{B} + \frac{\sigma^2 \text{tr}(\mathbf{H})}{B^2} \right). \quad (6)$$

By optimizing the learning rate η ², the per-sample, per-iteration improvement, $\max_{\eta} \Delta L_{\text{priv}}/B$, simplifies to

$$\Delta_{\text{priv}}^*(B) := \frac{1}{2} \frac{|\mathbf{G}|^4}{B\mathbf{G}^\top \mathbf{H} \mathbf{G} + \text{tr}(\mathbf{H}\Sigma) + \sigma^2 \text{tr}(\mathbf{H})/(Bc^2)}. \quad (7)$$

Given that the total number of processed samples is fixed at $S = BT$, (7) can be used as a metric to evaluate the *data efficiency* of different training settings, e.g. DP and non-DP training with different T, B and (ϵ, δ) .

Per-iteration improvement of vanilla SGD: According to Remark 2.2, we can analyze the loss improvement of standard SGD (which uses full public data) as a sub-case of DP-SGD by substituting $c = 1, \sigma = 0$ into (6). Additionally, we denote the batch size used for SGD and DP-SGD as $B_{\text{non-DP}}$ and B_{DP} , respectively:

$$\Delta L_{\text{pub}} := \eta \mathbf{G}^\top \mathbf{G} - \frac{\eta^2}{2} \left(\frac{\text{tr}(\mathbf{H}\Sigma)}{B_{\text{non-DP}}} + \mathbf{G}^\top \mathbf{H} \mathbf{G} \right). \quad (8)$$

Applying the optimal learning rate η , the per-sample per-iteration improvement $\max_{\eta} \Delta L_{\text{pub}}/B_{\text{non-DP}}$ is

$$\Delta_{\text{pub}}^*(B) := \frac{1}{2} \frac{|\mathbf{G}|^4}{B_{\text{non-DP}} \mathbf{G}^\top \mathbf{H} \mathbf{G} + \text{tr}(\mathbf{H}\Sigma)} \quad (9)$$

Implication 2.3 (Better DP mechanism helps). From (7), it is clear that smaller σ (from the advances in privacy accounting theory) and larger c (hence larger C_i) can help DP training. Under the same sensitivity bound, AUTO clipping gives the largest C_i among all clipping functions (see Figure 4), therefore is more preferred to use in practice.

Implication 2.4 (Moderately large batch size helps DP training). There exists an optimal batch size $B_{\text{DP}}^* := \text{argmax}_B \Delta_{\text{priv}}^*(B) \approx \sqrt{\frac{\sigma^2 \text{tr}(\mathbf{H})}{c^2 \mathbf{G}^\top \mathbf{H} \mathbf{G}}}$, as visualized in Figure 5. Compared to previous DP literatures, our derivation of B_{DP}^* also supports the use of large batch size, but further indicates the data inefficiency if B_{DP} is too large, a case that is often overlooked.

3 Impact of per-sample clipping and noising

In this section, we examine the effects of per-sample gradient clipping and noising on the DP training, leveraging the per-iteration per-sample loss improvement derived in Section 2. Specifically, we define and analyze a “**decelerator**” term that characterizes the slowdown by DP optimizers.

Comparing DP-SGD (7) to SGD (9), we can attribute the slow convergence of DP optimization to the term $\sigma^2 \text{tr}(\mathbf{H})/(Bc^2)$ in (7), which is not present in the standard training. We referred to such a term as the “decelerator”:

$$\text{decelerator: } \frac{\sigma^2 \text{tr}(\mathbf{H})}{Bc^2} \approx \frac{\sigma^2 \text{tr}(\mathbf{H}) \mathbb{E}|\mathbf{g}_i|^2}{B}, \quad (10)$$

which couples the effects of per-sample gradient clipping and noise through the trace of Hessian. We note that $\text{tr}(\mathbf{H})$ in (10) characterizes the curvature (i.e. sharpness or flatness) of the loss landscape, which strongly correlates with the downstream performance [50, 44, 94, 30].

Next, we discuss how the decelerator impacts the non-DP training, DP pre-training, and DP fine-tuning stages.

3.1 No noise, (almost) no deceleration

When $\sigma = 0$ (i.e., no DP noise), the decelerator vanishes and hence (7) reduces to (9), even if the per-sample gradient clipping is used. We empirically verified this in Figure 1 (see blue and black curves), where we see that the difference in convergence with or without clipping is negligible.

²The optimal learning rate of DP-SGD cannot be used in practice because (i) the oracle \mathbf{G} and \mathbf{H} are unknown; (ii) it is data-dependent and hence violates the DP guarantee. However, in our analysis such an optimal learning rate helps us understand the best possible per-iteration performance.

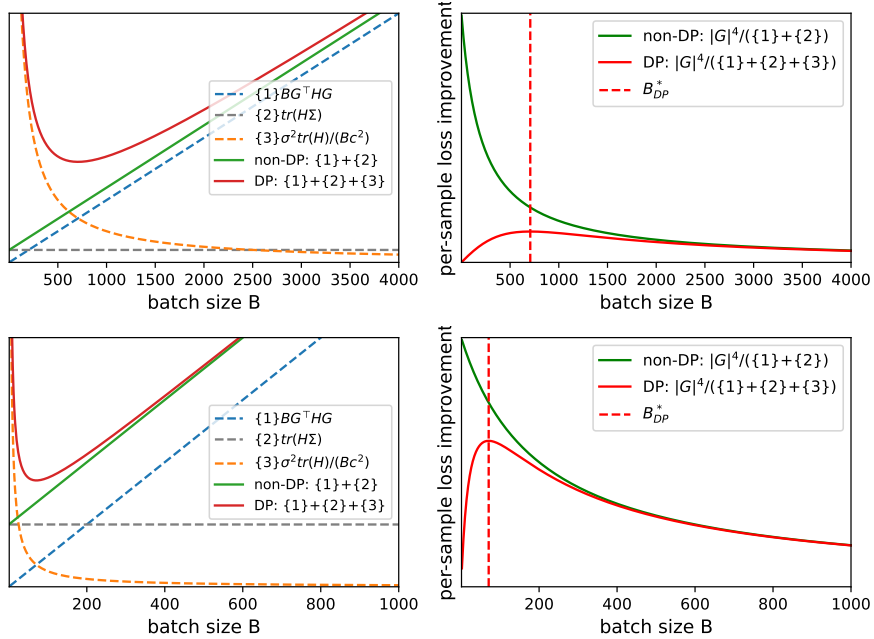


Figure 5: Illustration of different terms (7) for DP pre-training (upper) and DP fine-tuning (lower). Left sub-plots depict the denominator in (7).

3.2 DP pre-training can be vulnerable to noise

When $\sigma \neq 0$, the decelerator is non-zero. Therefore, DP training is slowed down by the noise; see Figure 1 that SGD with noise (yellow and red curves) has worse performance than SGD without noise (black and blue curves). Furthermore, in pre-training, the decelerator is relatively large in the denominator of (7), i.e., $B\mathbf{G}^\top\mathbf{H}\mathbf{G} + \text{tr}(\mathbf{H}\Sigma) \leq \frac{\sigma^2\text{tr}(\mathbf{H})}{Bc^2}$ unless B is large which is computationally inefficient (see Figure 5, upper left plot), and therefore, the slowdown can be significant.

Note that the deceleration issue cannot be resolved by increasing B . Although increasing B improves the relative (to non-DP) speed of DP convergence, i.e., the decelerator decreases, it hurts the absolute speed since $B\mathbf{G}^\top\mathbf{H}\mathbf{G}$ increases, and thus the loss improvement (7) also worsens (c.f. Figure 5 upper row). Therefore, to design an efficient DP pre-training strategy, we must keep B moderate and reduce the decelerator simultaneously.

3.3 DP fine-tuning is robust to noise

Empirical evidence has shown that DP fine-tuning is comparable to (though worse than) the standard fine-tuning [88, 48, 23, 57, 9, 11, 12], despite that $\sigma \neq 0$. Such a phenomenon implies that comparing public and DP finetuning, we have $\Delta_{\text{pub}}^*(B) \approx \Delta_{\text{priv}}^*(B)$; That is, the decelerator becomes small after the public pre-training. This is conceptually illustrated in Figure 5 (right column, say $B = 100$), where the DP curve is close to the non-DP curve at moderate B during fine-tuning, but not so during pre-training.

To understand the stark contrast between DP fine-tuning and DP pre-training, we plug in the optimal $B_{\text{DP}}^* = \sqrt{\frac{\sigma^2\text{tr}(\mathbf{H})}{c^2\mathbf{G}^\top\mathbf{H}\mathbf{G}}}$ from Implication 2.4 to $\Delta_{\text{priv}}^*(B)$. Then, we have the optimal improvement of DP-SGD as

$$\Delta_{\text{priv}}^*(B_{\text{DP}}^*) = \frac{1}{2} \frac{|\mathbf{G}|^4}{2\sqrt{\mathbf{G}^\top\mathbf{H}\mathbf{G}} \cdot \sigma^2\text{tr}(\mathbf{H})/c^2 + \text{tr}(\mathbf{H}\Sigma)}.$$

Notice that by choosing $B_{\text{non-DP}} = 2B_{\text{DP}}^*$, we have

$$\Delta_{\text{pub}}^*(2B_{\text{DP}}^*) = \Delta_{\text{priv}}^*(B_{\text{DP}}^*). \quad (11)$$

This indicates that DP-SGD with the optimal batch size is *as fast as* SGD with *twice* the batch size. Moreover, if B_{DP}^* is moderate, then DP-SGD can converge at similar speed to the SGD with optimal batch size.

Remark 3.1. From (9), we observe that non-DP training is data-efficient only if $B_{\text{non-DP}}\mathbf{G}^\top\mathbf{H}\mathbf{G} \ll \text{tr}(\mathbf{H}\Sigma)$, otherwise, we can decrease $B_{\text{non-DP}}$ to effectively improve Δ_{pub}^* . Therefore, by (11), DP training is data-efficient only if $B_{\text{DP}}^* = \frac{1}{2}B_{\text{non-DP}} \ll \frac{\text{tr}(\mathbf{H}\Sigma)}{2\mathbf{G}^\top\mathbf{H}\mathbf{G}}$, which holds in fine-tuning but not in early stage of pre-training (see Figure 6 right column, which illustrates the magnitude of the above three terms for pre-training and fine-tuning stages).

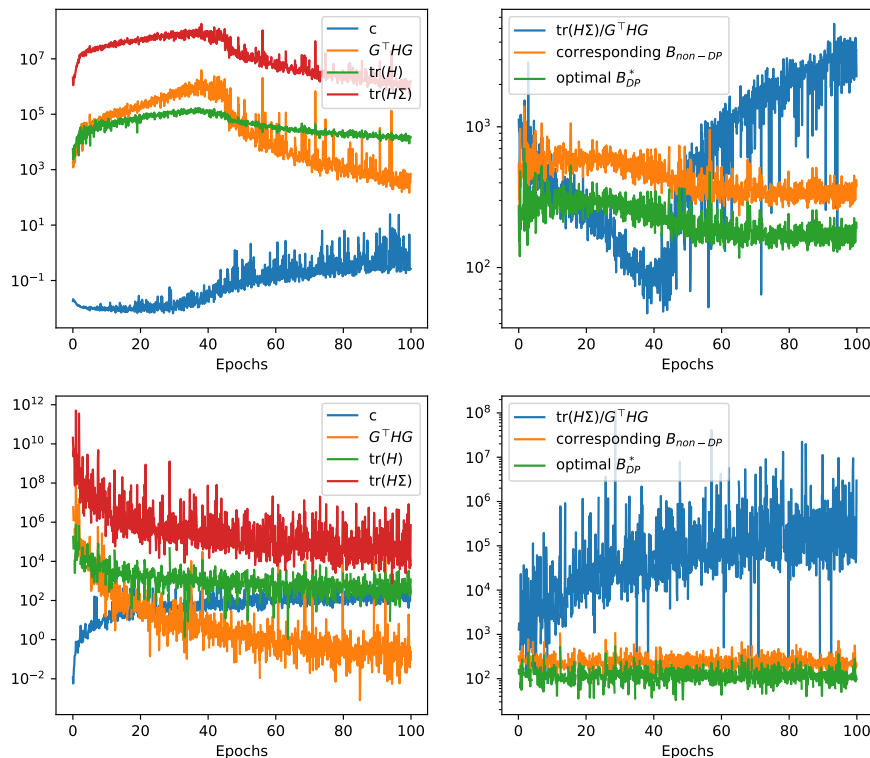


Figure 6: Evolution of terms in (7) and (9) that explains the deceleration of DP optimization, during pre-training (upper) and fine-tuning (lower) ViT-Base on CIFAR100.

3.4 Extension to general optimizers

The analysis in the previous two sections can be easily extended to arbitrary optimizers as well as techniques such as weight decay, gradient clipping, and parameter-efficient fine-tuning (PEFT). Let p be an optimizer’s post-processor of gradient and consider

$$\mathbf{w}_{t+1} = \mathbf{w}_t - \eta p(\mathbf{g}_t).$$

For examples, following the notation in Pytorch library [64], we can write Adam and SGD with momentum (μ) and weight decay (λ),

$$\text{Adam: } p(\mathbf{g}; \mathbf{m}, \mathbf{v}) = \frac{\frac{\beta_1 \mathbf{m} + (1 - \beta_1) \mathbf{g}}{1 - \beta_1^t}}{\sqrt{\frac{\beta_2 \mathbf{v} + (1 - \beta_2) \mathbf{g}^2}{1 - \beta_2^t} + 10^{-8}}}$$

$$\text{SGD}(\mu, \lambda): p(\mathbf{g}; \mathbf{b}, \mathbf{w}) = \mu \mathbf{b} + \mathbf{g} + \lambda \mathbf{w}.$$

Similarly, we can write any PEFT for any optimizer, e.g.

$$\text{PEFT (SGD): } p(\mathbf{g}; \mathbf{M}) = \mathbf{M} \odot \mathbf{g}$$

where $\mathbf{M} \in \{0, 1\}$ is an element-wise mask, with $\mathbf{M} = 0$ indicating that the parameter is non-trainable or frozen.

With respect to different $p(\cdot)$, the expected per-iteration loss improvement becomes

$$\Delta L(\eta) = \eta \mathbf{G}^\top \mathbb{E}[p(\mathbf{g})] - \frac{\eta^2}{2} \mathbb{E}[p(\mathbf{g})^\top \mathbf{H} p(\mathbf{g})]. \quad (12)$$

Applying Assumption 2.1 and the optimal learning rate, we can derive the expected per-sample per-iteration improvement, which is left in Appendix A.5 due to the complication in its form.

Specially, we consider optimizers such that $p(\cdot)$ is scale-invariant (i.e. $p(c\mathbf{G}) = p(\mathbf{G})$), such as SignSGD/Adam [4] or normalized SGD/LAMB [60, 54, 86].

Implication 3.2. Suppose the post-processor $p(\cdot)$ is scale-invariant. Denote $\mathbf{p} = p(\mathbf{G})$, $\mathbf{p}' = p'(\mathbf{G})$, the per-sample per-iteration improvement $\max_\eta \Delta L(\eta)/B$ simplifies to

$$\frac{1}{2} \frac{|\mathbf{p}^\top \mathbf{G}|^2}{B \mathbf{p}^\top \mathbf{H} \mathbf{p} + \text{tr}(\mathbf{p}'^\top \mathbf{H} \mathbf{p}' \boldsymbol{\Sigma}) + \sigma^2 \text{tr}(\mathbf{p}'^\top \mathbf{H} \mathbf{p}') / (Bc^2)}$$

Interestingly, similar to the decelerator of DP-SGD (10), the decelerator $\sigma^2 \text{tr}(\mathbf{p}'^\top \mathbf{H} \mathbf{p}') / (Bc^2)$ of these DP optimizers also couples the per-sample gradient clipping, the noise and the Hessian, rendering the theoretical implications from DP-SGD extendable to general DP optimizers.

4 Continual pre-training with DP

4.1 Necessity of public data in DP pre-training

In this section, we propose the DP continual pre-training strategy and demonstrate that the deceleration by DP can be effectively mitigated by using a certain amount of public data. We consider the mixed data training that uses both public data (with subscript $_0$ for related hyperparameters) and private data (with subscript $_1$). Then (4) becomes

$$\mathbf{g}_{\alpha,t} := \frac{\alpha_t}{B_0} \sum_{j \in \mathcal{B}_0} \mathbf{g}_{j,t} + \frac{(1 - \alpha_t)}{B_1} \left(\sum_{i \in \mathcal{B}_1} C_{i,t} \mathbf{g}_{i,t} + \sigma \mathcal{N}(0, \mathbf{I}_d) \right).$$

Here $\alpha_t \in [0, 1]$ controls the ratio of privatized and non-privatized gradients, taking different forms by public training (OnlyPublic, $\alpha_t = 1$), private training (OnlyPrivate, $\alpha_t = 0$), DPMD [2], a tunable constant [31, 51], and Sample [29, 43].

Table 2: Summary of α_t by mixed data training methods.

Ours	DPMD	Sample	OnlyPublic	OnlyPrivate
$\mathbb{I}(t < sT)$	$1 - \cos \frac{\pi t}{2K}$	$\frac{n_{\text{pub}}}{n_{\text{pub}} + n_{\text{priv}}}$	1	0

Using the mixed gradient \mathbf{g}_α and following (5), we can show that expected loss improvement is a bivariate quadratic function of (η, α) (see Appendix A.3). After minimizing with respect to both variables, we obtain:

$$\alpha^* = \left(\frac{1}{c} \frac{\text{tr}(\mathbf{H}\boldsymbol{\Sigma}) \cdot B_1/B_0}{\text{tr}(\mathbf{H}\boldsymbol{\Sigma}) + \sigma^2 \text{tr}(\mathbf{H}) / (B_1 c^2)} + 1 \right)^{-1} \quad (13)$$

Remark 4.1. From the optimal choice, we see $\alpha^* \neq 0$. It indicates that with the ability to access any public data ($\mathbf{g}_{j,t}$), the optimal improvement of mixed data training is larger than private training, i.e., $\Delta L_{\text{OnlyPrivate}}^* < \Delta L_{\text{mixed}}^*$.

Remark 4.2. Similarly, more private data also improves upon public training. The optimal $\alpha^* \neq 1$ also indicates that $\Delta L_{\text{OnlyPublic}}^* < \Delta L_{\text{mixed}}^*$ i.e., the improvement of mixed data training is larger than public training.

4.2 DP Continual pre-training strategy overview

Motivated by Section 3 and Remark 4.1, we propose a two-stage DP continual pre-training strategy: public pre-training for sT steps followed by private continual pre-training for $(1 - s)T$ steps, which is equivalent to setting $\alpha_t = \mathbb{I}(t < sT)$ and the constant $0 < s < 1$ controls the portion of steps of public training.

Table 3: Optimization by different training strategies.

	public data	private data	privacy
OnlyPublic	SGD	not used	Yes
OnlyPrivate	not used	DP-SGD	Yes
FullyPublic	SGD	SGD	No
FullyPrivate	DP-SGD	DP-SGD	Yes
Mixed (\mathbf{g}_α)	SGD	DP-SGD	Yes

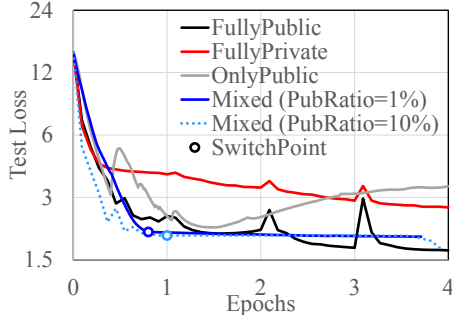


Figure 7: Convergence of GPT2-small on CodeParrot with different pre-training strategies ($\epsilon = 8$ if Mixed).

Remark 4.3. Although (13) suggests that $\alpha_t \in (0, 1)$, we only set binary $\alpha_t \in \{0, 1\}$ to avoid the difficulty of implementing two data loaders and two back-propagation mechanisms simultaneously (DP v.s. standard) in large optimization, e.g. memory and synchronization issues.

We highlight that DP continual pre-training is as distinct from DP fine-tuning as their non-DP counter-parts, despite both methods extending the learning from a pre-trained stage: the continual pre-training learns common knowledge without adapting to a specific task and serves a richer foundation for many downstream tasks (see more discussion in Appendix C). In fact, we show in Appendix A.8 that the loss improvement of DP continual pre-training can be almost as fast as non-DP pre-training (FullyPublic), thus closing the utility gap.

4.3 Technical Details: Stage Switching

We now demonstrate the technical details of our approach. **When to switch:** The switching, i.e. selecting s , can be automatically determined by public statistics without using any DP budget. For example, we can use early stopping based on the loss, i.e., switch after the loss on the validation dataset stops decreasing (see Figure 7, SwitchPoint of two Mixed training at different steps) or accuracy to switch to DP training. Alternatively, we can monitor $B_{\text{DP}}^* = \sqrt{\frac{\sigma^2 \text{tr}(\mathbf{H})}{c^2 \mathbf{G}^T \mathbf{H} \mathbf{G}}}$ and switch when it drops to the same level of $B_{\text{non-DP}}^*$, so that $\Delta_{\text{priv}}^* \approx \Delta_{\text{pub}}^*$.

How to switch Depending on whether the optimizer is scale-invariant, e.g. SGD v.s. Adam, the learning rate may need rescaling after switching to DP optimizers, in order to avoid training instability or even failure.

Suppose that on (10) is small, we recognize that DP-SGD needs to rescale the learning rate of SGD by $1/c$, where c is per-sample clipping factor. However, DP-Adam(SignSGD) and DP-LAMB do not need to. The proof of these facts is provided in Appendix A.6.

5 DP vision foundation models on ImageNet

We leverage the DP continual pre-training strategy discussed in Section 4 to train vision transformers [26] on ImageNet datasets. We use ImageNet-1k (1.3M images, 1k classes; [24]) for public pre-training, then ImageNet-11k (formally known as ImageNet-21k-P³, 11M images, 11k classes; [69]) for private pre-training. Notice that ImageNet-11k/21k is significantly harder to learn, with SOTA accuracy $\approx 47\%$ [69, 73] as compared to $> 85\%$ for ImageNet-1k. We apply data augmentation including random flip, contract shift, and rotation, and resizing to 224×224 . We evaluate our DP

³ImageNet-11k improves the dataset quality and thus the resulting models (see Table 3 in [69]), by removing the infrequent classes from the full ImageNet-21k, thus remaining 78% of its 14M images and 48% of 21.8k classes.

ViT on upstream and downstream tasks (including few-shot), achieving high accuracy under low computation budget (compared to existing DP pre-trained models in Table 4) while protecting the privacy of 90% training data.

5.1 Training strategy

For the public pre-training, we follow the self-supervised learning by [18] (self-distillation with no labels, or DINO), whereas the private continual pre-training is a supervised learning following [69]⁴. We employ AdamW optimizer with batch size $B = 4096$ and learning rate $\eta = 0.0002$ set by the line search⁵.

When automatically switching with early stopping (c.f. Section 4.3) from public to private pre-training, the classification head (the last layer) is re-initialized, after which we train with DP linear probing for 10 epochs then with DP full-parameter training for 20 epochs, with a total $\approx 100k$ training steps. This strategy achieves an upstream accuracy 41.5% on ImageNet-11k by our ViT-Base under $\epsilon = 8$, and 39.8% under $\epsilon = 2$.

5.2 Downstream performance

Our DP pre-training learns highly transferable representations, demonstrated through the strong performance on a list of downstream datasets. We summarize in Table 4 a number of models from previous literature for comparison. The most informative baselines are DINO and MIIL, since our DP models continue the pre-training from DINO, following the strategy of MIIL. Next, we mark **DP pre-trained models** in green and leave non-DP ones in black.

In Table 5, we compare different pre-training strategies (all non-DP except ours) leveraging the same dataset and same model architecture – ViT-Base (86M param). Our evaluation shows that DP pre-trained models achieve high downstream accuracy under standard and non-DP fine-tuning: 98.4% on CIFAR10, 90.2% on CIFAR100, 86.5% on Food101 and 96.8% on SVHN. Our DP continual pre-training clearly improves upon DINO, with $+0.3 \sim 2.0\%$ on accuracy, and is comparable to the non-DP pre-trained MIIL that uses twice the data size (1.4B v.s. our 0.7B).

In Table 6, when the downstream tasks (non-DP) are more challenging with only a few data samples to learn from, our DP model substantially outperforms previous DP pre-trained models across all settings, for example, by $+19 \sim 38\%$ on CIFAR100 when compared to ViP and TAN. We attribute the success to the high quality of pre-training

⁴We observe that, using augreg (a supervised pre-training strategy) for public pre-training on ImageNet-1k and/or ImageNet-21k for private pre-training gives very similar result.

⁵Our training strategy is similar to a concurrent work [89], with critical differences highlighted in Appendix C.

Table 4: Pre-training strategies of models. Standard non-DP training is marked in black; **DP training** is in green. † indicates self-supervised without using the labels. images \times is the total number of images used (dataset size \times epochs).

	reference	model	pre-training	continual training	non-privacy	images \times
TAN	[70]		ImageNet-1k	—	—	1.2B
(Syn)ViP	[89]	ViT-Base	Shaders21k [†]		Shaders21k	1.3B
ViP	[89]	ViT-Base	Shaders21k [†]	LAION400M[†]	Shaders21k	1.9B
DINO	[18]	ViT-Base	ImageNet-1k [†]	—	ImageNet-1k	0.3B
Ours	This work	ViT-Base	ImageNet-1k [†]	ImageNet-11k	ImageNet-1k	0.7B
MIIL	[69]	ViT-Base	ImageNet-1k	ImageNet-11k	ImageNet-11k	1.4B
Original	[26]	ViT-Base	ImageNet-21k	ImageNet-1k	ImageNet-21k	1.2B
AugReg	[73]	ViT-Base	ImageNet-1k	ImageNet-21k	ImageNet-21k	4.3B
NFnet-JFT	[23]	ResNet-50	JFT300M	—	JFT300M	4.0B

Table 5: Standard/DP fine-tuning accuracy with the same architecture (ViT-Base) and pre-training dataset (ImageNet-21k) up to subsampling and preprocessing. Number of processed images by each model is indicated in the parenthesis.

Fine-tuning Pre-training	CIFAR10			CIFAR100			Food101			SVHN		
	non-DP	$\epsilon = 8$	$\epsilon = 2$	non-DP	$\epsilon = 8$	$\epsilon = 2$	non-DP	$\epsilon = 8$	$\epsilon = 2$	non-DP	$\epsilon = 8$	$\epsilon = 2$
DINO (0.3B)	98.1	97.2	97.0	88.2	84.7	82.7	85.2	77.2	73.5	96.2	91.7	90.3
Ours$_{\epsilon=2}$ (0.7B)	97.8	96.6	96.1	88.8	83.1	81.1	84.8	75.5	72.5	96.3	91.3	90.1
Ours$_{\epsilon=8}$ (0.7B)	98.4	97.2	96.9	90.2	85.0	82.8	86.5	78.4	75.3	96.8	92.5	91.3
MIIL (1.4B)	98.8	98.5	98.2	91.4	90.9	89.2	87.2	84.5	83.0	96.8	93.3	92.0
ViT_base (1.2B)	98.9	98.3	98.1	92.6	89.9	88.2	89.4	85.5	83.1	96.9	93.5	92.5
AugReg (4.3B)	98.9	98.8	98.5	93.1	91.2	90.4	90.2	87.6	85.7	96.9	93.8	92.5

data, i.e. ImageNet-1k/11k, in contrast to Shaders (by comparing DINO to (Syn)ViP) and LAION (by comparing the improvement from DINO to ours and from (Syn)ViP to ViP).

Table 6: Few-shot accuracy of DP pre-trained models (TAN, ViP and ours) and their non-DP initialization.

	Aircraft (10-shot)	Aircraft (20-shot)	CIFAR100 (10-shot)	CIFAR100 (30-shot)	fine-tune epochs
TAN $_{\epsilon=8}$	22.84	37.93	27.78	42.35	200
(Syn)ViP	21.79	46.85	38.96	55.84	200
ViP $_{\epsilon=8}$	31.62	53.05	40.95	57.52	200
DINO	32.04	45.61	47.31	66.92	100
Ours $_{\epsilon=2}$	36.42	48.27	64.74	74.62	100
Ours $_{\epsilon=8}$	42.57	57.15	65.26	76.38	100

In Table 7, we extend the evaluation of full fine-tuning and linear probing to SOTA non-DP baselines and to million-image scale. Our DP model achieves 55.7% (+9.6% over ViP) on Places365 with 1.8M images and 60.0% (+21.9% over ViP) on iNat2021 with 2.7M images. The current non-DP SOTA is 57-60% on Places365 [23, 26] and about 64% on iNat2021 [78, 59] after pre-training on 2.7 ~ 4B images. This showcases the effectiveness of DP pre-training (only leveraging 0.7B images).

Table 7: Linear-probing accuracy (non-DP) of pre-trained models, except “full” indicating full-parameter. For ImageNet-1k (seen in our pre-training), it is only meaningful to compare our models to DINO and observe the benefit of continual pre-training, but not to others.

	ImageNet-1k	Places365	iNat2021	fine-tune epochs
# images	1M	1.8M	2.7M	
TAN $_{\epsilon=8}$	49.0	40.5	31.7	90 / 90 / 90
(Syn)ViP	49.8	43.2	32.4	90 / 90 / 90
ViP $_{\epsilon=8}$	55.7	46.1	38.1	90 / 90 / 90
DINO	76.1	52.1	43.5	8 / 5 / 10
Ours $_{\epsilon=2}$	76.2	52.5	46.5	8 / 5 / 10
Ours $_{\epsilon=8}$	77.9	53.0	49.1	8 / 5 / 10
Ours $_{\epsilon=2}$ (full)	78.0	55.6	57.2	8 / 5 / 10
Ours $_{\epsilon=8}$ (full)	78.5	55.7	60.0	8 / 5 / 10
NFnet-JFT	74.1	54.5	—	10 / 26 / —

5.3 Privacy protection

We employ a white-box membership inference attack (MIA) to evaluate the data protection by our DP pre-training: 1) for each image in ImageNet-11k, we compute its output logits and loss, which serves as the feature of the MIA dataset; 2) we randomly select 50% of the testing images and the same number of training images (522, 496 samples) as the MIA test set, and the rest data as MIA train set; 3) we label the training images as class “1” and testing images as class “0”. This creates the MIA dataset with 11k features and binary labels.

We fit a logistic regression with the MIA training set to classify whether an image belongs to the training set of ImageNet-11k (class “1”) or not. We report the results on the MIA testing set in Table 8, showing the effectiveness of DP protection when $\epsilon \leq 8$.

Table 8: Membership inference attack results. Values closer to 0.5 indicate better privacy protection.

	Accuracy	Precision	Recall	F1	AUC
Ours $_{\epsilon=2}$	50.1%	50.1%	47.5%	0.49	0.50
Ours $_{\epsilon=8}$	51.3%	51.6%	64.4%	0.57	0.51
Ours $_{\epsilon=\infty}$	53.8%	54.1%	71.2%	0.62	0.54
MIL	54.0%	58.5%	77.3%	0.67	0.62

6 Discussion

In this paper, we conduct an insightful and unified convergence analysis on DP optimization. Specifically, we identify the decelerator (10) of DP training as a result of the per-sample gradient clipping, the noise and the Hessian, which can be significantly mitigated by a small amount ($< 10\%$) of public training. Consequently, we propose DP continual pre-training to enrich a foundation model’s knowledge via the private data. We are excited to demonstrate that, on large-scale systems, our DP pre-training is almost as accurate and implementable as the fully public pre-training.

References

- [1] Martin Abadi, Andy Chu, Ian Goodfellow, H Brendan McMahan, Ilya Mironov, Kunal Talwar, and Li Zhang. Deep learning with differential privacy. In *Proceedings of the 2016 ACM SIGSAC conference on computer and communications security*, pages 308–318, 2016.
- [2] Ehsan Amid, Arun Ganesh, Rajiv Mathews, Swaroop Ramaswamy, Shuang Song, Thomas Steinke, Vinith M Suriyakumar, Om Thakkar, and Abhradeep Thakurta. Public data-assisted mirror descent for private model training. In *International Conference on Machine Learning*, pages 517–535. PMLR, 2022.
- [3] Raef Bassily, Adam Smith, and Abhradeep Thakurta. Private empirical risk minimization: Efficient algorithms and tight error bounds. In *Proceedings of the 2014 IEEE 55th Annual Symposium on Foundations of Computer Science*, pages 464–473, 2014.
- [4] Jeremy Bernstein, Yu-Xiang Wang, Kamyar Aizzadenesheli, and Animashree Anandkumar. signsgd: Compressed optimisation for non-convex problems. In *International Conference on Machine Learning*, pages 560–569. PMLR, 2018.
- [5] Leonard Berrada, Soham De, Judy Hanwen Shen, Jamie Hayes, Robert Stanforth, David Stutz, Pushmeet Kohli, Samuel L Smith, and Borja Balle. Unlocking accuracy and fairness in differentially private image classification. *arXiv preprint arXiv:2308.10888*, 2023.
- [6] Tom Brown, Benjamin Mann, Nick Ryder, Melanie Subbiah, Jared D Kaplan, Prafulla Dhariwal, Arvind Nee-lakantan, Pranav Shyam, Girish Sastry, Amanda Askell, et al. Language models are few-shot learners. *Advances in neural information processing systems*, 33:1877–1901, 2020.
- [7] Zhiqi Bu, Jinshuo Dong, Qi Long, and Weijie J Su. Deep learning with gaussian differential privacy. *Harvard data science review*, 2020(23), 2020.
- [8] Zhiqi Bu, Ruixuan Liu, Yu-Xiang Wang, Sheng Zha, and George Karypis. On the accuracy and efficiency of group-wise clipping in differentially private optimization. *arXiv preprint arXiv:2310.19215*, 2023.
- [9] Zhiqi Bu, Jialin Mao, and Shiyun Xu. Scalable and efficient training of large convolutional neural networks with differential privacy. *Advances in Neural Information Processing Systems*, 35:38305–38318, 2022.
- [10] Zhiqi Bu, Hua Wang, Zongyu Dai, and Qi Long. On the convergence and calibration of deep learning with differential privacy. *Transactions on Machine Learning Research*, 2023.
- [11] Zhiqi Bu, Yu-Xiang Wang, Sheng Zha, and George Karypis. Automatic clipping: Differentially private deep learning made easier and stronger. *arXiv preprint arXiv:2206.07136*, 2022.
- [12] Zhiqi Bu, Yu-Xiang Wang, Sheng Zha, and George Karypis. Differentially private bias-term only fine-tuning of foundation models. In *Workshop on Trustworthy and Socially Responsible Machine Learning, NeurIPS 2022*, 2022.
- [13] Zhiqi Bu, Yu-Xiang Wang, Sheng Zha, and George Karypis. Differentially private optimization on large model at small cost. In *International Conference on Machine Learning*, pages 3192–3218. PMLR, 2023.
- [14] Zhiqi Bu and Yuan Zhang. Differentially private optimizers can learn adversarially robust models. *Transactions on Machine Learning Research*, 2023.

- [15] Nicholas Carlini, Steve Chien, Milad Nasr, Shuang Song, Andreas Terzis, and Florian Tramer. Membership inference attacks from first principles. In *2022 IEEE Symposium on Security and Privacy (SP)*, pages 1897–1914. IEEE, 2022.
- [16] Nicholas Carlini, Daphne Ippolito, Matthew Jagielski, Katherine Lee, Florian Tramer, and Chiyuan Zhang. Quantifying memorization across neural language models. In *The Eleventh International Conference on Learning Representations*, 2022.
- [17] Nicholas Carlini, Florian Tramer, Eric Wallace, Matthew Jagielski, Ariel Herbert-Voss, Katherine Lee, Adam Roberts, Tom Brown, Dawn Song, Ulfar Erlingsson, et al. Extracting training data from large language models. In *30th USENIX Security Symposium (USENIX Security 21)*, pages 2633–2650, 2021.
- [18] Mathilde Caron, Hugo Touvron, Ishan Misra, Hervé Jégou, Julien Mairal, Piotr Bojanowski, and Armand Joulin. Emerging properties in self-supervised vision transformers. In *Proceedings of the IEEE/CVF international conference on computer vision*, pages 9650–9660, 2021.
- [19] Junjie Chen, Wendy Hui Wang, and Xinghua Shi. Differential privacy protection against membership inference attack on machine learning for genomic data. In *BIOCOMPUTING 2021: Proceedings of the Pacific Symposium*, pages 26–37. World Scientific, 2020.
- [20] Xiangyi Chen, Steven Z Wu, and Mingyi Hong. Understanding gradient clipping in private sgd: A geometric perspective. *Advances in Neural Information Processing Systems*, 33:13773–13782, 2020.
- [21] Mike Conover, Matt Hayes, Ankit Mathur, Jianwei Xie, Jun Wan, Sam Shah, Ali Ghodsi, Patrick Wendell, Matei Zaharia, and Reynold Xin. Free dolly: Introducing the world’s first truly open instruction-tuned llm, 2023.
- [22] Rudrajit Das, Abolfazl Hashemi, Sujay Sanghavi, and Inderjit S Dhillon. On the convergence of differentially private federated learning on non-lipschitz objectives, and with normalized client updates. *arXiv preprint arXiv:2106.07094*, 2021.
- [23] Soham De, Leonard Berrada, Jamie Hayes, Samuel L Smith, and Borja Balle. Unlocking high-accuracy differentially private image classification through scale. *arXiv preprint arXiv:2204.13650*, 2022.
- [24] Jia Deng, Wei Dong, Richard Socher, Li-Jia Li, Kai Li, and Li Fei-Fei. Imagenet: A large-scale hierarchical image database. In *2009 IEEE conference on computer vision and pattern recognition*, pages 248–255. Ieee, 2009.
- [25] Jinshuo Dong, Aaron Roth, and Weijie J Su. Gaussian differential privacy. *arXiv preprint arXiv:1905.02383*, 2019.
- [26] Alexey Dosovitskiy, Lucas Beyer, Alexander Kolesnikov, Dirk Weissenborn, Xiaohua Zhai, Thomas Unterthiner, Mostafa Dehghani, Matthias Minderer, Georg Heigold, Sylvain Gelly, et al. An image is worth 16x16 words: Transformers for image recognition at scale. In *International Conference on Learning Representations*, 2020.
- [27] Jingfei Du, Édouard Grave, Beliz Gunel, Vishrav Chaudhary, Onur Celebi, Michael Auli, Veselin Stoyanov, and Alexis Conneau. Self-training improves pre-training for natural language understanding. In *Proceedings of the 2021 Conference of the North American Chapter of the Association for Computational Linguistics: Human Language Technologies*, pages 5408–5418, 2021.
- [28] Cynthia Dwork, Frank McSherry, Kobbi Nissim, and Adam Smith. Calibrating noise to sensitivity in private data analysis. In *Theory of cryptography conference*, pages 265–284. Springer, 2006.
- [29] Cecilia Ferrando, Jennifer Gillenwater, and Alex Kulesza. Combining public and private data. *arXiv preprint arXiv:2111.00115*, 2021.
- [30] Pierre Foret, Ariel Kleiner, Hossein Mobahi, and Behnam Neyshabur. Sharpness-aware minimization for efficiently improving generalization. In *International Conference on Learning Representations*, 2020.
- [31] Aditya Golatkar, Alessandro Achille, Yu-Xiang Wang, Aaron Roth, Michael Kearns, and Stefano Soatto. Mixed differential privacy in computer vision. *arXiv preprint arXiv:2203.11481*, 2022.

- [32] Ian J Goodfellow, Jonathon Shlens, and Christian Szegedy. Explaining and harnessing adversarial examples. *arXiv preprint arXiv:1412.6572*, 2014.
- [33] Sivakanth Gopi, Yin Tat Lee, and Lukas Wutschitz. Numerical composition of differential privacy. *Advances in Neural Information Processing Systems*, 34, 2021.
- [34] Chuan Guo, Geoff Pleiss, Yu Sun, and Kilian Q Weinberger. On calibration of modern neural networks. In *International conference on machine learning*, pages 1321–1330. PMLR, 2017.
- [35] Suchin Gururangan, Ana Marasović, Swabha Swayamdipta, Kyle Lo, Iz Beltagy, Doug Downey, and Noah A Smith. Don’t stop pretraining: Adapt language models to domains and tasks. In *Proceedings of the 58th Annual Meeting of the Association for Computational Linguistics*, pages 8342–8360, 2020.
- [36] Moritz Hardt, Eric Price, and Nati Srebro. Equality of opportunity in supervised learning. *Advances in neural information processing systems*, 29, 2016.
- [37] Jiyang He, Xuechen Li, Da Yu, Huishuai Zhang, Janardhan Kulkarni, Yin Tat Lee, Arturs Backurs, Nenghai Yu, and Jiang Bian. Exploring the limits of differentially private deep learning with group-wise clipping. *arXiv preprint arXiv:2212.01539*, 2022.
- [38] Kaiming He, Xiangyu Zhang, Shaoqing Ren, and Jian Sun. Deep residual learning for image recognition. In *Proceedings of the IEEE conference on computer vision and pattern recognition*, pages 770–778, 2016.
- [39] Shlomo Hoory, Amir Feder, Avichai Tendler, Sofia Erell, Alon Peled-Cohen, Itay Laish, Hootan Nakhost, Uri Stemmer, Ayelet Benjamini, Avinatan Hassidim, et al. Learning and evaluating a differentially private pre-trained language model. In *Findings of the Association for Computational Linguistics: EMNLP 2021*, pages 1178–1189, 2021.
- [40] Daniel Huynh. Starcoder memorization experiment highlights privacy risks of fine-tuning on code. <https://huggingface.co/blog/dhuynh95/starcoder-memorization-experiment>, 2023.
- [41] Huseyin A Inan, Osman Ramadan, Lukas Wutschitz, Daniel Jones, Victor Rühle, James Withers, and Robert Sim. Training data leakage analysis in language models. *arXiv preprint arXiv:2101.05405*, 2021.
- [42] Shaoxiong Ji, Tianlin Zhang, Kailai Yang, Sophia Ananiadou, Erik Cambria, and Jörg Tiedemann. Domain-specific continued pretraining of language models for capturing long context in mental health. *arXiv preprint arXiv:2304.10447*, 2023.
- [43] Zach Jorgensen, Ting Yu, and Graham Cormode. Conservative or liberal? personalized differential privacy. In *2015 IEEE 31st international conference on data engineering*, pages 1023–1034. IEEE, 2015.
- [44] Nitish Shirish Keskar, Dheevatsa Mudigere, Jorge Nocedal, Mikhail Smelyanskiy, and Ping Tak Peter Tang. On large-batch training for deep learning: Generalization gap and sharp minima. In *International Conference on Learning Representations*, 2016.
- [45] Diederik P Kingma and Jimmy Ba. Adam: A method for stochastic optimization. *arXiv preprint arXiv:1412.6980*, 2014.
- [46] Alexey Kurakin, Steve Chien, Shuang Song, Roxana Geambasu, Andreas Terzis, and Abhradeep Thakurta. Toward training at imagenet scale with differential privacy. *arXiv preprint arXiv:2201.12328*, 2022.
- [47] Xuechen Li, Daogao Liu, Tatsunori B Hashimoto, Huseyin A Inan, Janardhan Kulkarni, Yin-Tat Lee, and Abhradeep Guha Thakurta. When does differentially private learning not suffer in high dimensions? *Advances in Neural Information Processing Systems*, 35:28616–28630, 2022.
- [48] Xuechen Li, Florian Tramèr, Percy Liang, and Tatsunori Hashimoto. Large language models can be strong differentially private learners. *arXiv preprint arXiv:2110.05679*, 2021.
- [49] Chin-Yew Lin. Rouge: A package for automatic evaluation of summaries. In *Text summarization branches out*, pages 74–81, 2004.

- [50] Hong Liu, Sang Michael Xie, Zhiyuan Li, and Tengyu Ma. Same pre-training loss, better downstream: Implicit bias matters for language models. In *International Conference on Machine Learning*, pages 22188–22214. PMLR, 2023.
- [51] Ruixuan Liu, Zhiqi Bu, Yu-xiang Wang, Sheng Zha, and George Karypis. Coupling public and private gradient provably helps optimization. *arXiv preprint arXiv:2310.01304*, 2023.
- [52] Nils Lukas, Ahmed Salem, Robert Sim, Shruti Tople, Lukas Wutschitz, and Santiago Zanella-Béguelin. Analyzing leakage of personally identifiable information in language models. In *2023 IEEE Symposium on Security and Privacy (SP)*, pages 346–363. IEEE Computer Society, 2023.
- [53] Yi-An Ma, Teodor Vanislavov Marinov, and Tong Zhang. Dimension independent generalization of dp-sgd for overparameterized smooth convex optimization. *arXiv preprint arXiv:2206.01836*, 2022.
- [54] Danilo P Mandic. A generalized normalized gradient descent algorithm. *IEEE signal processing letters*, 11(2):115–118, 2004.
- [55] Stephan Mandt, Matthew D Hoffman, and David M Blei. Stochastic gradient descent as approximate bayesian inference. *Journal of Machine Learning Research*, 18:1–35, 2017.
- [56] Sam McCandlish, Jared Kaplan, Dario Amodei, and OpenAI Dota Team. An empirical model of large-batch training. *arXiv preprint arXiv:1812.06162*, 2018.
- [57] Harsh Mehta, Abhradeep Thakurta, Alexey Kurakin, and Ashok Cutkosky. Large scale transfer learning for differentially private image classification. *arXiv preprint arXiv:2205.02973*, 2022.
- [58] Ilya Mironov. Rényi differential privacy. In *2017 IEEE 30th computer security foundations symposium (CSF)*, pages 263–275. IEEE, 2017.
- [59] Andre Nakkab, Benjamin Feuer, and Chinmay Hegde. Lit tuned models for efficient species detection. In *2nd AAAI Workshop on AI for Agriculture and Food Systems*, 2023.
- [60] Yurii Nesterov. *Introductory lectures on convex optimization: A basic course*, volume 87. Springer Science & Business Media, 2003.
- [61] Lily Hay Newman and Andy Greenberg. Chatgpt spit out sensitive data when told to repeat ‘poem’ forever. <https://www.wired.com/story/chatgpt-poem-forever-security-roundup/>, 2023.
- [62] Nicolas Papernot, Abhradeep Thakurta, Shuang Song, Steve Chien, and Ulfar Erlingsson. Tempered sigmoid activations for deep learning with differential privacy.
- [63] Kishore Papineni, Salim Roukos, Todd Ward, and Wei jing Zhu. Bleu: a method for automatic evaluation of machine translation. pages 311–318, 2002.
- [64] Adam Paszke, Sam Gross, Soumith Chintala, Gregory Chanan, Edward Yang, Zachary DeVito, Zeming Lin, Alban Desmaison, Luca Antiga, and Adam Lerer. Automatic differentiation in pytorch. 2017.
- [65] Natalia Ponomareva, Hussein Hazimeh, Alex Kurakin, Zheng Xu, Carson Denison, H Brendan McMahan, Sergei Vassilvitskii, Steve Chien, and Abhradeep Guha Thakurta. How to dp-fy ml: A practical guide to machine learning with differential privacy. *Journal of Artificial Intelligence Research*, 77:1113–1201, 2023.
- [66] Katyanna Quach. Inside the 1tb imagenet data set used to train the world’s ai: Naked kids, drunken frat parties, porno stars, and more, Oct 2019.
- [67] Alec Radford, Jeffrey Wu, Rewon Child, David Luan, Dario Amodei, Ilya Sutskever, et al. Language models are unsupervised multitask learners.
- [68] Md Atiqur Rahman, Tanzila Rahman, Robert Laganière, Noman Mohammed, and Yang Wang. Membership inference attack against differentially private deep learning model. *Trans. Data Priv.*, 11(1):61–79, 2018.

- [69] Tal Ridnik, Emanuel Ben-Baruch, Asaf Noy, and Lihi Zelnik-Manor. Imagenet-21k pretraining for the masses. In *Thirty-fifth Conference on Neural Information Processing Systems Datasets and Benchmarks Track (Round 1)*, 2021.
- [70] Tom Sander, Pierre Stock, and Alexandre Sablayrolles. Tan without a burn: Scaling laws of dp-sgd. In *International Conference on Machine Learning*, pages 29937–29949. PMLR, 2023.
- [71] Dezhao Song, Andrew Vold, Kanika Madan, and Frank Schilder. Multi-label legal document classification: A deep learning-based approach with label-attention and domain-specific pre-training. *Information Systems*, 106:101718, 2022.
- [72] Shuang Song, Thomas Steinke, Om Thakkar, and Abhradeep Thakurta. Evading the curse of dimensionality in unconstrained private glms. In *International Conference on Artificial Intelligence and Statistics*, pages 2638–2646. PMLR, 2021.
- [73] Andreas Steiner, Alexander Kolesnikov, Xiaohua Zhai, Ross Wightman, Jakob Uszkoreit, and Lucas Beyer. How to train your vit? data, augmentation, and regularization in vision transformers. *arXiv preprint arXiv:2106.10270*, 2021.
- [74] Rohan Taori, Ishaan Gulrajani, Tianyi Zhang, Yann Dubois, Xuechen Li, Carlos Guestrin, Percy Liang, and Tatsunori B. Hashimoto. Stanford alpaca: An instruction-following llama model. https://github.com/tatsu-lab/stanford_alpaca, 2023.
- [75] Hugo Touvron, Thibaut Lavril, Gautier Izacard, Xavier Martinet, Marie-Anne Lachaux, Timothée Lacroix, Baptiste Rozière, Naman Goyal, Eric Hambro, Faisal Azhar, et al. Llama: Open and efficient foundation language models. *arXiv preprint arXiv:2302.13971*, 2023.
- [76] Florian Tramer and Dan Boneh. Differentially private learning needs better features (or much more data). *arXiv preprint arXiv:2011.11660*, 2020.
- [77] Florian Tramèr, Gautam Kamath, and Nicholas Carlini. Considerations for differentially private learning with large-scale public pretraining. *arXiv preprint arXiv:2212.06470*, 2022.
- [78] Grant Van Horn, Elijah Cole, Sara Beery, Kimberly Wilber, Serge Belongie, and Oisín Mac Aodha. Benchmarking representation learning for natural world image collections. In *Proceedings of the IEEE/CVF conference on computer vision and pattern recognition*, pages 12884–12893, 2021.
- [79] Di Wang, Changyou Chen, and Jinhui Xu. Differentially private empirical risk minimization with non-convex loss functions. In *International Conference on Machine Learning*, pages 6526–6535. PMLR, 2019.
- [80] Di Wang and Jinhui Xu. Differentially private empirical risk minimization with smooth non-convex loss functions: A non-stationary view. In *Proceedings of the AAAI Conference on Artificial Intelligence*, volume 33, pages 1182–1189, 2019.
- [81] Zihan Wang, K Karthikeyan, Stephen Mayhew, and Dan Roth. Extending multilingual bert to low-resource languages. In *Findings of the Association for Computational Linguistics: EMNLP 2020*, pages 2649–2656, 2020.
- [82] Kang Wei, Jun Li, Ming Ding, Chuan Ma, Howard H Yang, Farhad Farokhi, Shi Jin, Tony QS Quek, and H Vincent Poor. Federated learning with differential privacy: Algorithms and performance analysis. *IEEE Transactions on Information Forensics and Security*, 15:3454–3469, 2020.
- [83] Zeke Xie, Issei Sato, and Masashi Sugiyama. A diffusion theory for deep learning dynamics: Stochastic gradient descent exponentially favors flat minima. In *International Conference on Learning Representations*, 2020.
- [84] Xiaodong Yang, Huishuai Zhang, Wei Chen, and Tie-Yan Liu. Normalized/clipped sgd with perturbation for differentially private non-convex optimization. *arXiv preprint arXiv:2206.13033*, 2022.
- [85] Jiayuan Ye, Zhenyu Zhu, Fanghui Liu, Reza Shokri, and Volkan Cevher. Initialization matters: Privacy-utility analysis of overparameterized neural networks. *arXiv preprint arXiv:2310.20579*, 2023.

- [86] Yang You, Jing Li, Sashank Reddi, Jonathan Hseu, Sanjiv Kumar, Srinadh Bhojanapalli, Xiaodan Song, James Demmel, Kurt Keutzer, and Cho-Jui Hsieh. Large batch optimization for deep learning: Training bert in 76 minutes. In *International Conference on Learning Representations*, 2019.
- [87] Ashkan Yousefpour, Igor Shilov, Alexandre Sablayrolles, Davide Testuggine, Karthik Prasad, Mani Malek, John Nguyen, Sayan Ghosh, Akash Bharadwaj, Jessica Zhao, Graham Cormode, and Ilya Mironov. Opacus: User-friendly differential privacy library in PyTorch. *arXiv preprint arXiv:2109.12298*, 2021.
- [88] Da Yu, Saurabh Naik, Arturs Backurs, Sivakanth Gopi, Huseyin A Inan, Gautam Kamath, Janardhan Kulkarni, Yin Tat Lee, Andre Manoel, Lukas Wutschitz, et al. Differentially private fine-tuning of language models. *arXiv preprint arXiv:2110.06500*, 2021.
- [89] Yaodong Yu, Maziar Sanjabi, Yi Ma, Kamalika Chaudhuri, and Chuan Guo. Vip: A differentially private foundation model for computer vision. *arXiv preprint arXiv:2306.08842*, 2023.
- [90] Guodong Zhang, Lala Li, Zachary Nado, James Martens, Sushant Sachdeva, George Dahl, Chris Shallue, and Roger B Grosse. Which algorithmic choices matter at which batch sizes? insights from a noisy quadratic model. *Advances in neural information processing systems*, 32, 2019.
- [91] Xinwei Zhang, Xiangyi Chen, Mingyi Hong, Zhiwei Steven Wu, and Jinfeng Yi. Understanding clipping for federated learning: Convergence and client-level differential privacy. In *International Conference on Machine Learning, ICML 2022*, 2022.
- [92] Yingxue Zhou, Steven Wu, and Arindam Banerjee. Bypassing the ambient dimension: Private sgd with gradient subspace identification. In *International Conference on Learning Representations*, 2020.
- [93] Zhanxing Zhu, Jingfeng Wu, Bing Yu, Lei Wu, and Jinwen Ma. The anisotropic noise in stochastic gradient descent: Its behavior of escaping from sharp minima and regularization effects. *arXiv preprint arXiv:1803.00195*, 2018.
- [94] Zhanxing Zhu, Jingfeng Wu, Bing Yu, Lei Wu, and Jinwen Ma. The anisotropic noise in stochastic gradient descent: Its behavior of escaping from sharp minima and regularization effects. In *International Conference on Machine Learning*, pages 7654–7663. PMLR, 2019.

A Derivation and proofs

A.1 Derivation of Equation (5)

$$\begin{aligned}
\Delta L &:= \eta \mathbf{G}^\top \mathbb{E}[\mathbf{g}] - \frac{\eta^2}{2} \mathbb{E}[\mathbf{g}^\top \mathbf{H} \mathbf{g}] \\
&\stackrel{(a)}{=} \eta \mathbf{G}^\top \mathbb{E}[\mathbf{g}] - \frac{\eta^2}{2} \text{tr}(\mathbf{H} \mathbb{E}[\mathbf{g} \mathbf{g}^\top]) \\
&\stackrel{(b)}{=} \eta \mathbf{G}^\top \mathbb{E}[\mathbf{g}] - \frac{\eta^2}{2} \text{tr}(\mathbf{H} \text{Cov}(\mathbf{g})) + \text{tr}(\mathbf{H} \mathbb{E}[\mathbf{g}] \mathbb{E}[\mathbf{g}]^\top) \\
&\stackrel{(c)}{=} \eta \mathbf{G}^\top \mathbb{E}[\mathbf{g}] - \frac{\eta^2}{2} (\text{tr}(\mathbf{H} \text{Cov}(\mathbf{g})) + \mathbb{E}[\mathbf{g}]^\top \mathbf{H} \mathbb{E}[\mathbf{g}])
\end{aligned}$$

where (a) uses equations (16) and then (15) to the second term; (b) separates the expectation of $\mathbf{g} \mathbf{g}^\top$ into its mean squared and covariance and uses (14); (c) uses equations (15) and then (16) to the last term.

Property of the trace:

$$\text{tr}(\mathbf{A} + \mathbf{B}) = \text{tr}(\mathbf{A}) + \text{tr}(\mathbf{B}), \quad \text{tr}(c\mathbf{A}) = c \text{tr}(\mathbf{A}), \quad \text{Linearity,} \quad (14)$$

$$\text{tr}(\mathbf{AB}) = \text{tr}(\mathbf{BA}), \quad \text{Trace of product,} \quad (15)$$

$$\text{tr}(a) = a, \quad \text{Trace of a number.} \quad (16)$$

A.2 Explanation for Implication 2.4

We will leverage GDP to validate that $\sigma(B)^2/B \approx O(1/B)$, given that most of other privacy accountants are numerical and hard to interpret. We note that μ -GDP has an one-to-one mapping with the (ϵ, δ) -DP:

$$\delta = \Phi\left(-\frac{\epsilon}{\mu} + \frac{\mu}{2}\right) + \Phi\left(-\frac{\epsilon}{\mu} - e^{\frac{\epsilon}{\mu}}\right)$$

where Φ is the normal cumulative distribution function.

Lemma A.1. *Given an iterative algorithm with ℓ_2 sensitivity 1 at each iteration, which uniformly samples the data in dataset of size n with ratio $\frac{B}{n}$, by injecting Gaussian noise $\mathcal{N}(0, \sigma^2 \mathbf{I})$ to the output of the algorithm at each iteration, it satisfies μ -GDP with*

$$\mu = \frac{B}{n} \sqrt{T(e^{1/\sigma(B)^2} - 1)} = \sqrt{BS(e^{1/\sigma(B)^2} - 1)/n},$$

where S denotes the fixed computation budget.

The proof is equivalent to that in Section 2.4 in [25].

By Taylor expansion,

$$\sigma(B)^2 = \frac{1}{\log\left(\frac{\mu^2 n^2}{BS} + 1\right)} = \frac{BS}{\mu^2 n^2} + \frac{1}{2} + O\left(\frac{1}{B}\right) \rightarrow \frac{\sigma(B)^2}{B} = \frac{S}{\mu^2 n^2} + \frac{1}{2B} + o\left(\frac{1}{B}\right)$$

In the pre-training regime, S/n is the number of epochs (usually between 1 and 300) and the sample size n is huge, i.e. $n > 10^7$ for ImageNet and $n > 10^9$ for large language model training. Hence the first term is negligible and $\sigma(B)^2/B \approx 0.5B$.

A.3 Proof of results in Section 3.3

Proof. Leveraging (2), we have

$$\begin{aligned}
\mathbb{E}(\mathbf{g}) &= \alpha \mathbf{G} + (1 - \alpha)c\mathbf{G}, \quad \text{Cov}(\mathbf{g}) \\
&= \alpha^2 \frac{\boldsymbol{\Sigma}}{B_0} + (1 - \alpha)^2 \left(\frac{c^2 \boldsymbol{\Sigma}}{B_1} + \frac{\sigma^2 \mathbf{I}}{B_1^2} \right)
\end{aligned}$$

Substituting in the mixed gradient \mathbf{g}_α and following (5), we can write down the expected improvement of mixed data training:

$$\begin{aligned}\Delta L_{\text{mixed}} &= \eta(\alpha + (1 - \alpha)c)\mathbf{G}^\top \mathbf{G} - \frac{\eta^2(1 - \alpha)^2\sigma^2}{2B_1^2}\text{tr}(\mathbf{H}) \\ &\quad - \frac{\eta^2}{2}\left(\frac{\alpha^2}{B_0} + \frac{(1 - \alpha)^2}{B_1}c^2\right)\text{tr}(\mathbf{H}\Sigma) \\ &\quad - \frac{\eta^2}{2}(\alpha + (1 - \alpha)c)^2\mathbf{G}^\top \mathbf{H}\mathbf{G},\end{aligned}$$

which is a bivariate quadratic function ΔL_{mixed} to be minimized over (η, α) . To make the presentation easier, we denote $\eta_0 = \eta\alpha, \eta_1 = \eta(1 - \alpha)$, and the above equation can be rewritten as:

$$\Delta L_{\text{mixed}} = (\eta_1 c + \eta_0)\mathbf{G}^\top \mathbf{G} - \frac{1}{2}\frac{\eta_1^2\sigma^2}{B_1^2}\text{tr}(\mathbf{H}) - \frac{1}{2}\left(\frac{\eta_1^2}{B_1}c^2 + \frac{\eta_0^2}{B_0}\right)\text{tr}(\mathbf{H}\Sigma) - \frac{1}{2}(\eta_1 c + \eta_0)^2\mathbf{G}^\top \mathbf{H}\mathbf{G}.$$

Note that if we set $\eta_1 = 0$ or $\eta_0 = 0$, we essentially train the model with only public data or private data, respectively. can be written as a bivariate quadratic function over (η_0, η_1) :

$$\Delta L_{\text{mixed}} = -(A\eta_0^2 + B\eta_1^2 + C\eta_0 + D\eta_1 + E\eta_0\eta_1)$$

in which

$$\begin{aligned}A &= \frac{1}{2}\mathbf{G}^\top \mathbf{H}\mathbf{G} + \frac{1}{2}\frac{\text{tr}(\mathbf{H}\Sigma)}{B_0}, \\ B &= \frac{1}{2}c^2\mathbf{G}^\top \mathbf{H}\mathbf{G} + \frac{1}{2}c^2\frac{\text{tr}(\mathbf{H}\Sigma)}{B_1} + \frac{1}{2}\frac{\sigma^2\text{tr}(\mathbf{H})}{B_1^2}, \\ C &= -\mathbf{G}^\top \mathbf{G}, \\ D &= -c\mathbf{G}^\top \mathbf{G}, \\ E &= c\mathbf{G}^\top \mathbf{H}\mathbf{G}.\end{aligned}$$

The maximizer is

$$\eta_0 = -\frac{2BC - DE}{4AB - E^2}, \eta_1 = -\frac{2AD - CE}{4AB - E^2}.$$

Hence

$$\frac{1 - \alpha^*}{\alpha^*} = \frac{2AD - CE}{2BC - DE} \implies \alpha^* = 1 / \left(\frac{2AD - CE}{2BC - DE} + 1 \right)$$

Finally

$$\alpha^* = \left(\frac{\text{ctr}(\mathbf{H}\Sigma)\mathbf{G}^\top \mathbf{G}/B_0}{c^2\text{tr}(\mathbf{H}\Sigma)\mathbf{G}^\top \mathbf{G}/B_1 + \sigma^2\text{tr}(\mathbf{H})\mathbf{G}^\top \mathbf{G}/B_1^2} + 1 \right)^{-1} = \left(\frac{1}{c} \frac{\text{tr}(\mathbf{H}\Sigma) \cdot B_1/B_0}{\text{tr}(\mathbf{H}\Sigma) + \sigma^2\text{tr}(\mathbf{H})/(B_1c^2)} + 1 \right)^{-1}$$

□

A.4 Explanation of Remark 3.1

From (7), the optimal batch size for DP-SGD is

$$\arg \max_B \frac{1}{2} \frac{|\mathbf{G}|^4}{B\mathbf{G}^\top \mathbf{H}\mathbf{G} + \text{tr}(\mathbf{H}\Sigma) + \sigma^2\text{tr}(\mathbf{H})/(Bc^2)} = \arg \min_B B\mathbf{G}^\top \mathbf{H}\mathbf{G} + \text{tr}(\mathbf{H}\Sigma) + \sigma^2\text{tr}(\mathbf{H})/(Bc^2) \approx \sqrt{\frac{\sigma^2\text{tr}(\mathbf{H})}{c^2\mathbf{G}^\top \mathbf{H}\mathbf{G}}}$$

which minimizes (7) to

$$\text{DP-SGD}(B_{\text{DP}}^*) \longrightarrow \frac{1}{2} \frac{|\mathbf{G}|^4}{2\sqrt{\mathbf{G}^\top \mathbf{H}\mathbf{G} \cdot \sigma^2\text{tr}(\mathbf{H})/c^2} + \text{tr}(\mathbf{H}\Sigma)}$$

where $B_{\text{DP}}^* := \sqrt{\frac{\sigma^2\text{tr}(\mathbf{H})}{c^2\mathbf{G}^\top \mathbf{H}\mathbf{G}}}$.

Note this is equivalent to applying $B_{\text{non-DP}} := 2\sqrt{\frac{\sigma^2 \text{tr}(\mathbf{H})}{c^2 \mathbf{G}^\top \mathbf{H} \mathbf{G}}} = 2B_{\text{DP}}^*$ on (9),

$$\text{SGD}(B_{\text{non-DP}}) \equiv \text{SGD}(2B_{\text{DP}}^*) \equiv \text{DP-SGD}(B_{\text{DP}}^*).$$

We emphasize that generally

$$\text{SGD}(2B_{\text{DP}}) \not\equiv \text{DP-SGD}(B_{\text{DP}}).$$

A.5 Loss improvement of general DP optimizers – Implication 3.2

From (12), the expected per-iteration loss improvement becomes

$$\Delta L = \eta \mathbf{G}^\top \mathbb{E}[p(\mathbf{g})] - \frac{\eta^2}{2} (\text{tr}(\mathbf{H} \text{Cov}(p(\mathbf{g}))) + \mathbb{E}[p(\mathbf{g})]^\top \mathbf{H} \mathbb{E}[p(\mathbf{g})]). \quad (17)$$

Applying Assumption 2.1 and delta method, with $\mathbf{G} = \frac{\partial L}{\partial \mathbf{w}}$, we have

$$\sqrt{B}(p(\mathbf{g}) - p(c\mathbf{G})) = \sqrt{B}p'(c\mathbf{G}) \cdot (\mathbf{g} - c\mathbf{G}) + o_p(1) \rightarrow \mathcal{N}(0, p'(c\mathbf{G})[c^2\boldsymbol{\Sigma} + \sigma^2/B]p'(c\mathbf{G})^\top)$$

where $p'(c\mathbf{G}) \equiv \frac{\partial p(c\mathbf{G})}{\partial c\mathbf{G}} \in \mathbb{R}^{d \times d}$. Hence

$$\mathbb{E}(p(\mathbf{g})) \approx p(c\mathbf{G}), \text{Cov}(p(\mathbf{g})) \approx p'(c\mathbf{G}) \cdot (c^2\boldsymbol{\Sigma}/B + \sigma^2/B^2) \cdot p'(c\mathbf{G})^\top$$

Next, the expected improvement contributed by one sample is a quadratic function of η :

$$\Delta L/B \approx \left(\eta p(c\mathbf{G})^\top \mathbf{G} - \frac{\eta^2}{2} \frac{\sigma^2 \text{tr}[p'(c\mathbf{G})^\top \mathbf{H} p'(c\mathbf{G})]}{B^2} - \frac{\eta^2}{2} \frac{c^2 \text{tr}[p'(c\mathbf{G})^\top \mathbf{H} p'(c\mathbf{G}) \boldsymbol{\Sigma}]}{B} - \frac{\eta^2}{2} p(c\mathbf{G})^\top \mathbf{H} p(c\mathbf{G}) \right) / B$$

Applying the optimal learning rate, the optimal per-sample loss improvement $\Delta L/B$ at each iteration simplifies to

$$\frac{1}{2} \frac{|p(c\mathbf{G})^\top \mathbf{G}|^2}{B p(c\mathbf{G})^\top \mathbf{H} p(c\mathbf{G}) + c^2 \text{tr}(p'(c\mathbf{G})^\top \mathbf{H} p'(c\mathbf{G}) \boldsymbol{\Sigma}) + \sigma^2 \text{tr}(p'(c\mathbf{G})^\top \mathbf{H} p'(c\mathbf{G})) / B}$$

In the special case that p is scale-invariant, e.g. in adaptive optimizers like Adam or in SignSGD, we get $p'(c\mathbf{G}) = \frac{\partial p(c\mathbf{G})}{\partial c\mathbf{G}} = \frac{\partial p(\mathbf{G})}{\partial \mathbf{G}} \frac{\partial \mathbf{G}}{\partial c\mathbf{G}} = p'(\mathbf{G})/c$ and thus

$$\frac{1}{2} \frac{|p(\mathbf{G})^\top \mathbf{G}|^2}{B p(\mathbf{G})^\top \mathbf{H} p(\mathbf{G}) + \text{tr}(p'(\mathbf{G})^\top \mathbf{H} p'(\mathbf{G}) \boldsymbol{\Sigma}) + \sigma^2 \text{tr}(p'(\mathbf{G})^\top \mathbf{H} p'(\mathbf{G})) / (Bc^2)}$$

A.6 Proof of Section 4.3

Proof. We can write down the optimal learning rate for DP-SGD from (7),

$$\eta_{\text{DP-SGD}}^* = \frac{1}{c} \frac{|\mathbf{G}|^2}{\mathbf{G}^\top \mathbf{H} \mathbf{G} + \text{tr}(\mathbf{H} \boldsymbol{\Sigma})/B + \sigma^2 \text{tr}(\mathbf{H}) / (Bc)^2}, \quad (18)$$

and that for the standard SGD is

$$\eta_{\text{SGD}}^* = \frac{|\mathbf{G}|^2}{\mathbf{G}^\top \mathbf{H} \mathbf{G} + \text{tr}(\mathbf{H} \boldsymbol{\Sigma})/B} \approx \frac{|\mathbf{G}|^2}{\mathbf{G}^\top \mathbf{H} \mathbf{G} + \text{tr}(\mathbf{H} \boldsymbol{\Sigma})/B + \sigma^2 \text{tr}(\mathbf{H}) / (Bc)^2}, \quad (19)$$

given that the decelerator is small. It is obvious that a factor of $\frac{1}{c}$ is multiplied when switching from SGD to DP-SGD.

Denote SI for scale-invariant optimizers, we can write down the optimal learning rate from Implication 3.2,

$$\eta_{\text{SI}}^* = \frac{|\mathbf{p}^\top \mathbf{G}|}{B \mathbf{p}^\top \mathbf{H} \mathbf{p} + \text{tr}(\mathbf{p}'^\top \mathbf{H} \mathbf{p}' \boldsymbol{\Sigma}) + \sigma^2 \text{tr}(\mathbf{p}'^\top \mathbf{H} \mathbf{p}') / (Bc^2)}, \quad (20)$$

We note that there is no factor of $\frac{1}{c}$ when setting $\sigma = 0, c = 1$ for non-DP optimizers. \square

optimization	performance		example
L	L	vanilla	L is cross-entropy
L	L_{other}	vanilla	L is cross-entropy; L_{other} is BLEU or accuracy
L_{mod}	L	adversarial training	L_{mod} is adversarial loss; L is cross-entropy

Table 9: DP/non-DP optimization when the optimization loss is different to the performance measures.

A.7 Improvement of performance measures other than the optimization loss

We now consider two extended cases when the optimization loss is different to the performance measures. For example, the model may be trained via the cross-entropy loss but measured on 0-1 accuracy.

For the first case, we analyze many performance measures of DP models (denoted as L_{other}) beyond the optimization loss L . For instance, foundation models trained on cross-entropy loss can be evaluated on classification accuracy, F1 score, BLEU [63], ROGUE [49], fairness [36], calibration [34], adversarial robustness, etc.

We demonstrate that our analysis in previous sections indeed generalizes: equivalent to (6), we have

$$\Delta L_{\text{other}}(\eta) = \eta \mathbf{G}_{\text{other}}^\top \mathbb{E}[\mathbf{g}] - \frac{\eta^2}{2} \mathbb{E}[\mathbf{g}^\top \mathbf{H}_{\text{other}} \mathbf{g}]$$

where $\mathbf{G}_{\text{other}}, \mathbf{H}_{\text{other}}$ are the oracle gradient and Hessian of L_{other} . The per-sample per-iteration improvement, $\max_{\eta} \Delta L_{\text{other}}/B$, simplifies to

$$\frac{1}{2} \frac{|\mathbf{G}_{\text{other}}^\top \mathbf{G}|^2}{B \mathbf{G}^\top \mathbf{H}_{\text{other}} \mathbf{G} + \text{tr}(\mathbf{H}_{\text{other}} \boldsymbol{\Sigma}) + \sigma^2 \text{tr}(\mathbf{H}_{\text{other}})/(Bc^2)},$$

with the decelerator being $\sigma^2 \text{tr}(\mathbf{H}_{\text{other}})/(Bc^2)$ in place of (10). As implied by Section 3.3, we expect the public pre-training also mitigates this decelerator, so that well-trained DP models and non-DP models should be equally performant. Empirically speaking, DP fine-tuning has shown to be as accurate [48, 23], adversarially robust [14], calibrated [10], and fair [5] as the standard fine-tuning.

For the second case, e.g. adversarial, sharpness-aware, fairness-aware or calibration-aware training, the optimization is on the modified loss $\frac{\partial L_{\text{mod}}}{\partial \mathbf{w}}$ but the performance is measured on the vanilla loss $\frac{\partial L}{\partial \mathbf{w}}$. For instance, we want an adversarially trained model to be sufficiently accurate. To be specific, FGSM and PGD (L_2/L_∞ perturbation with norm ρ) lead to the modified loss

$$L_{\text{mod}} := \max_{\|\xi\| \leq \rho} \mathbb{E}_x[L(\mathbf{w}, x + \xi)], \mathbf{G}_{\text{mod}} = \frac{\partial L_{\text{mod}}}{\partial \mathbf{w}}.$$

DP adversarial training applies on

$$\mathbf{p} = \frac{1}{B} \left(\sum_i C_i \mathbf{g}_{\text{mod},i} + \sigma \mathcal{N}(0, \mathbf{I}_d) \right) \approx \frac{1}{B} \left(c \sum_i \mathbf{g}_{\text{mod},i} + \sigma \mathcal{N}(0, \mathbf{I}_d) \right)$$

where per-sample gradient is $\mathbf{g}_{\text{mod},i} := \frac{\partial \max_{\|\xi\| \leq \rho} L(\mathbf{w}, x_i + \xi)}{\partial \mathbf{w}}$. Note that the modified gradient may be post-processed by optimizers like AdamW as in (12). To be clear, only in this section, we write $\mathbf{p} = \frac{\partial L_{\text{mod}}}{\partial \mathbf{w}}$ and omit the post-processing of the optimizer (i.e. we only show for SGD).

Next, the expected per-iteration loss improvement becomes

$$\Delta L = \eta \mathbf{G}^\top \mathbb{E}[\mathbf{p}] - \frac{\eta^2}{2} (\text{tr}(\mathbf{H} \text{Cov}(\mathbf{p})) + \mathbb{E}[\mathbf{p}]^\top \mathbf{H} \mathbb{E}[\mathbf{p}]). \quad (21)$$

Applying Assumption 2.1, we have

$$\mathbb{E}[\mathbf{p}] = c \mathbf{G}_{\text{mod}}, \text{Cov}(\mathbf{p}) = c^2 \boldsymbol{\Sigma}_{\text{mod}}/B + \sigma^2/B^2$$

Hence, the expected per-iteration improvement contributed by one sample is a quadratic function of η :

$$\Delta L/B := (\eta c \mathbf{G}^\top \mathbf{G}_{\text{mod}} - \frac{\eta^2}{2} \frac{\sigma^2 \text{tr}(\mathbf{H})}{B^2} - \frac{\eta^2}{2} \frac{c^2 \text{tr}(\mathbf{H} \boldsymbol{\Sigma}_{\text{mod}})}{B} - \frac{\eta^2}{2} c^2 \mathbf{G}_{\text{mod}}^\top \mathbf{H} \mathbf{G}_{\text{mod}})/B$$

Applying the optimal learning rate, the optimal per-sample per-iteration improvement, $\max_{\eta} \Delta L/B$, simplifies to

$$\frac{1}{2} \frac{|\mathbf{G}^\top \mathbf{G}_{\text{mod}}|^2}{B \mathbf{G}_{\text{mod}}^\top \mathbf{H} \mathbf{G}_{\text{mod}} + \text{tr}(\mathbf{H} \boldsymbol{\Sigma}_{\text{mod}}) + \sigma^2 \text{tr}(\mathbf{H}) / (Bc^2)} \quad (22)$$

Again, the decelerator is the same as (10). Therefore, DP training will be as good as the standard training when the decelerator is small under the modified loss. This supports the observation that DP adversarial training can be accurate in [14], if DP natural training is comparable to non-DP natural training.

A.8 Explaining the effectiveness of DP continual pre-training

Taking a step further than Remark 4.1, we claim that DP continual pre-training can converge as fast as non-DP pre-training (FullyPublic), conditioning on that the non-DP initialization is sufficiently strong: running sT iterations of public training followed by the DP training is only marginally weaker than FullyPublic in (9):

$$\begin{aligned} & \sum_{t=1}^{sT} \frac{|\mathbf{G}_t|^4}{\mathbf{G}_t^\top \mathbf{H}_t \mathbf{G}_t + \frac{\text{tr}(\mathbf{H}_t \boldsymbol{\Sigma}_t)}{B}} + \sum_{t=sT}^T \frac{|\mathbf{G}_t|^4}{\mathbf{G}_t^\top \mathbf{H}_t \mathbf{G}_t + \frac{\text{tr}(\mathbf{H}_t \boldsymbol{\Sigma}_t)}{B}} + (10) \\ & \approx \sum_{t=1}^{sT} \frac{|\mathbf{G}_t|^4}{\mathbf{G}_t^\top \mathbf{H}_t \mathbf{G}_t + \frac{\text{tr}(\mathbf{H}_t \boldsymbol{\Sigma}_t)}{B}} + \sum_{t=sT}^T \frac{|\mathbf{G}_t|^4}{\mathbf{G}_t^\top \mathbf{H}_t \mathbf{G}_t + \frac{\text{tr}(\mathbf{H}_t \boldsymbol{\Sigma}_t)}{B}}, \end{aligned}$$

given that the decelerator (10) is small for $t > sT$.

B Experiment settings and additional details

In this section, we provide additional descriptions and experiment details for the numerical results in the main paper.

B.1 Datasets

We use the following datasets throughout this paper.

- ImageNet: ImageNet-21k [24] is the full dataset with various releases which contain 14.2M images from 21,841 classes. ImageNet-1k is a subset of ImageNet-21k using 1k high-level classes. We use the ILSVRC2012 version, which contains 1.2 million training images and 100000 test images. ImageNet-11k [69] is another subset of ImageNet-21k that removes invalid/infrequent classes, retaining 11.1M images (train:test=10.5M :0.52M) and 10,450 classes in the Winter21 version.
- CIFAR-10/CIFAR-100: 50,000 training and 10,000 test images, with 10 or 100 classes, respectively.
- Food101: it contains 101 classes of food, with 101,000 images in total, 1000 images per class (training 750 and test 250).
- SVHN: it contains 10 classes of digits in natural scene images, with 73257 training and 26032 test images.
- Aircraft: FGVC Aircraft dataset contains 3334 training and 3333 test images with 100 classes.
- Places365: Places365-Standard dataset contains 1.8 million training and 36000 test images from 365 scene classes.
- iNat2021: iNaturalist 2021 dataset contains 10,000 classes of species, with 2.7 million training and 0.1 million test images.
- CodeParrot: a GitHub dataset of about 180 GB containing roughly 20 million Python files. We use 3% of these files, that is 606,720 rows of training and 3322 rows of test data. We take sequence length 128.
- E2E: a dataset of restaurant reviews, containing 42,061 training and 4693 test instances. We take sequence length 100.

B.2 Experiment settings

For images, we use 224×224 resolution and patch 16 for vision transformers.

B.2.1 Figure 1

We use batch size 1000 and search over learning rate $\in [5e-5, 1e-4, 2e-4, 5e-4]$.

1. CIFAR10, ViT-Base, random initialization, $\eta = 5e-5$ without noise, $\eta = 5e-4$ with noise, 10 epochs.
2. CIFAR100, ViT-Large, pretrained by `timm` library, $\eta = 5e-5$ without noise, $\eta = 5e-4$ with noise, 5 epochs.
3. CodeParrot, GPT2-Large, random initialization, $\eta = 1e-4$ without clipping, $\eta = 5e-4$ with clipping. This follows closely from <https://huggingface.co/learn/nlp-course/chapter7/6>.
4. E2E, GPT2-Large, pretrained by `transformers` library, $\eta = 1e-4$ without noise, $\eta = 5e-4$ with noise, 10 epochs.

B.2.2 Figure 3

$n = 10^6, \epsilon = 1, \delta = 1/n, S = 10^6$ (1 epoch). We use the privacy accountants in Opacus [87]: RDP [58], GDP [25, 7], PRV [33]. The dashed lines depict $\sigma(1)^2/B$ for these privacy accountants.

B.2.3 Figure 5

For pre-training, $\sigma^2 = 0.25, \mathbf{G}^\top \mathbf{H} \mathbf{G} = 1e2, \text{tr}(\mathbf{H})/c^2 = 2e8, \text{tr}(\mathbf{H}\Sigma) = 2e4$; for fine-tuning, $\sigma^2 = 0.25, \mathbf{G}^\top \mathbf{H} \mathbf{G} = 1e2, \text{tr}(\mathbf{H})/c^2 = 2e6, \text{tr}(\mathbf{H}\Sigma) = 2e4$.

B.2.4 Figure 6

We train ViT-Base with $\eta = 5e-4, B = 500, \epsilon = 2$. We use the Hutchinson method to compute Hessian-related trace, e.g. $\text{tr}(\mathbf{H}) = \mathbb{E}_{\mathbf{v} \in \mathbb{R}^d}[\mathbf{v}^\top \mathbf{H} \mathbf{v}] \leftarrow \frac{1}{k} \sum_{i=1}^k \mathbf{v}_i^\top \mathbf{H} \mathbf{v}_i$, where $\mathbf{v} \sim N(0, I_d)$ and $k = 100$. Note the Hessian-vector product $\mathbf{H} \mathbf{v}$ can be computed by one back-propagation of $\mathbf{G}(\mathbf{w})^\top \mathbf{v} \in \mathbb{R}$ on \mathbf{w} .

B.2.5 Figure 7

We train GPT2-small with $\eta = 2 \times 10^{-4}, B = 7680$, epochs $E_{\text{pub}} = 1$ (if not early stopped by patience = 2), $E_{\text{priv}} = 3$ for mixed training, $E = 4$ for other cases. In the figure, ‘PubRatio’ is the percentage of public data among all data.

B.2.6 Table 5

We empirically observe that ViT-Base models with/without fine-tuning on ImageNet1k.

E.g. `vit_base_patch16_224_miil_in21k_ft_in1k` v.s. `vit_base_patch16_224_miil_in21k`;

`vit_base_patch16_224_augreg_in21k_ft_in1k` v.s. `vit_base_patch16_224_augreg_in21k` are very similar in final accuracy, though those with fine-tuning converge faster at early epochs.

We train for 10 epochs, $B = 1000$.

- non-DP fine-tuning: full-parameter, $\eta = 5e-5$ (except for SVHN and CIFAR10 under $\epsilon = 2$, we use $\eta = 2e-5$ instead).
- DP fine-tuning: BiTFiT [12], $\eta = 2e-3$ (except for SVHN and CIFAR10 under $\epsilon = 2$, we use $\eta = 5e-4$ instead). We observe that for our models, the accuracy may benefit from a smaller learning rate (1e-3) when $\epsilon \geq 8$.

B.2.7 Table 6

We train with full-parameter fine-tuning and $B = 1000$. Our learning rate $\eta = 5e-5$ ($\epsilon = 8$) and $\eta = 2e-5$ ($\epsilon = 2$). x -shot means x samples per class, e.g. 30-shot CIFAR100 means 3000 samples in total.

B.2.8 Table 7

We train with $\eta = 5e - 5$ ($\epsilon = 8$) and $\eta = 2e - 5$ ($\epsilon = 2$) for full-parameter fine-tuning and parameter-efficient fine-tuning. We note that with much heavier (public) pre-training, e.g. on JFT4B, DP NFnet-F3 and JFT4B can achieve even better accuracy [23].

B.3 Details in training stage switching

When switching from public pre-training to private continual pre-training, the DP gradient may have a different scale than the historical optimizer states and make the continual pre-training unstable. Therefore, we investigate different strategies to re-initialize the optimizer states during the switching. Throughout the training, we use AdamW, which have three states: the iteration index (t), the first-order momentum (\mathbf{m}), and the second-order momentum (\mathbf{v}).

In the experiment, we train a ViT-Base model from scratch on the CIFAR100 dataset. In the first three epochs, we use vanilla AdamW, then we switch to DP-AdamW and continue training for one epoch. During the switching, we fixed the learning rate as suggested by Section 4.3 and reset different states ($t, \mathbf{v}, \mathbf{m}$) to zeros. The ablation study result is shown in Figure 8.

From the figure, we observe that re-initializing the first-order momentum \mathbf{m} (R1) results in the best performance when switching from public to private training. For the other cases, we observe a performance drop when switching.

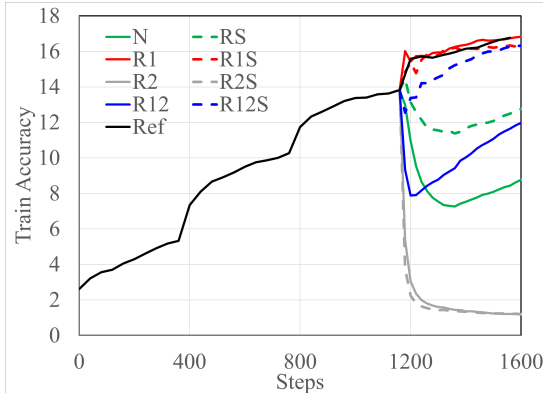


Figure 8: Ablation study of switching from non-DP to DP training with AdamW on CIFAR100 dataset. When switching ($T = 1200$), we re-initialize different states in the AdamW optimizer in different linestyles. “R1”, “R2”, and “RS” indicate \mathbf{m} , \mathbf{v} and t are re-initialized, respectively. “N” indicates no re-initialization, and “Ref” is the reference behavior of continual training with non-DP AdamW.

B.4 Details for MIA

To conduct the membership inference attack (MIA) in Table 8, we employ a white-box attack with full access to model parameters and data, to evaluate the data protection by our DP pre-training. The attack has two major steps. **Step I: construct MIA dataset.** To construct the MIA dataset, we use the following procedures: 1) for each image in ImageNet-11k, we compute its output logits and loss, which serves as the feature of the MIA dataset; 2) we randomly select 50% of the testing images and the same number of training images (522, 496 samples) as the MIA test set, and the rest 50% of the testing images and 10% of the training images as MIA train set; 3) we label the training images as class “1” and testing images as class “0”. This creates the MIA dataset with 11k features and binary labels. **Step II: evaluate MIA performance.** After obtaining the MIA dataset, we fit a binary logistic regression with the MIA training set to classify whether an image belongs to the training set of ImageNet-11k (class “1”). We use the L-BFGS optimizer and class re-weighting to train the model for 50 epochs. After training, we evaluate the performance of the training classification model on the MIA test dataset and compute the classification accuracy, precision, recall, F1-score, and AUROC of the classification task. The MIA attack procedures are illustrated in Figure 9.

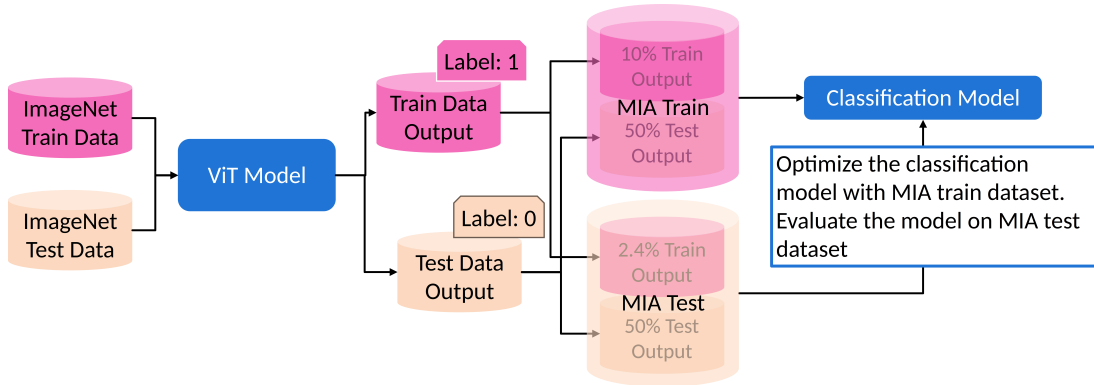


Figure 9: The process of membership inference attack (MIA).

C Related works

Convergence analysis of DP training (the goals) Recent works have attributed the slow DP convergence to the large number of model parameters [92, 47], the noise level added to gradients [82, 11, 84], and the per-sample gradient clipping [10, 20, 91]. Our analysis in (7) and (10) covers these factors as well as the choice of hyperparameters. We note that a key quantity of DP convergence is $\text{tr}(\mathbf{H})$, which implicitly covers the model dimension d and is also analyzed in [53] to give a dimension-free generalization bound. Moreover, existing works mostly study the empirical convergence on the training set, in terms of the gradient norm $\|\mathbf{g}_t\| \rightarrow 0$, the parameter space $\mathbf{w}_t \rightarrow \mathbf{w}_*$, or the training loss $L_t \rightarrow L_*$ as $t \rightarrow \infty$. Our work focuses on the *generalization* performance, and pays particular attention on the *data efficiency* (as well as computation efficiency) that is rarely captured in the literature.

More on DP convergence analysis (the assumptions) The convergence analysis of non-convex DP deep learning is very challenging and under-studied. There are roughly 3 routes to walk around the challenge: (1) Working on convex models instead (see [72, 22] and more in Sec 4.1.2 [65]), e.g. assuming some form of convexity or only optimizing the last layer (essentially a linear model). This route offers deep theoretical insights thanks to the simplified models, but generally fails to match the training dynamics nor the performance of deep learning. For instance, last-layer training may work reasonably well in computer vision but not so in language tasks, obtaining only 26 BLEU score for DP-GPT2 on E2E dataset compared to 63 BLEU score via DP full-parameter training. (2) Working on the continuous-time gradient flow, rather than the gradient descent in practice, in order to get around the per-sample gradient clipping [85] or the Gaussian noise [10]. This route essentially works with infinitely small learning rate, which falls short in the performance as SOTA DP models are trained with large learning rate [48]. (3) Assuming that the loss L is Lipschitz continuous (i.e. the gradient is bounded) [3, 79, 80] or Lipschitz smooth [20, 11, 84]. While both assumptions lead to some insights of the DP training behaviors, the Lipschitz constant is hardly calculable and time-dependent (maybe even diverging) in practice. Particularly, in the Lipschitz continuous setting, the per-sample gradient clipping is not used in DP deep learning, reducing the technical difficulty significantly but missing the gist of DP-SGD from a practitioner’s viewpoint.

In contrast, our work does not rely on these and many other assumptions in the literature, because we do not study the loss convergence along all iterations. We instead scrutinize the per-iteration loss improvement in (6). Put differently, we focus on the local behavior of DP optimizer rather than the global behavior.

Differentially private training The literature of DP deep learning has predominantly focused on fine-tuning the pre-trained models (e.g. full-parameter [1, 48, 11] and PEFT [76, 88, 12, 57]). Importantly, DP fine-tuning (1) can be as performant as the standard non-DP fine-tuning consistently, (2) achieves better empirical performance with larger models [11, 8] and (3) necessarily relies on the public data pre-training. Our work is distinct from previous works since we focus on DP pre-training with large sample size, large number of iterations, and very limited public data (c.f. Table 1 and next paragraph for the difference between fine-tuning and continual pre-training). Interestingly, we notice that DP pre-training also enjoy these desirable characteristics of DP fine-tuning, e.g. requiring public data (only a small amount) in Section 4.1 and benefiting from scaling up the models (see Figure 4, Figure 5 and Table 9 in [89]). This empirical evidence of similar training dynamics between DP pre-training and DP fine-tuning, despite their

difference in learning goals, is well-supported by our decelerator analysis in Section 3.

Continual pre-training Continual pre-training is a training strategy that accumulates knowledge from a large amount of data, in order to improve its generalization ability to unseen domains and datasets [35, 27, 81, 42, 71]. It is different from fine-tuning which focuses on a task-specific and often smaller dataset. Therefore, the (continually) pre-trained models possess strong few-shot (including zero-shot) ability but may not be competent in specific functionality such as conversation, and vice versa for fine-tuned models like ChatGPT, Alpaca [74], and Dolly [21].

Multiple DP pre-trained models have been developed [46, 23, 89], but these models either (1) suffer from low accuracy, e.g. 6.9% on ImageNet-1k without additional data by [46] and 32.4% by [23]; or (2) demand significantly more data and compute to match the non-DP pre-training, e.g. $100\times$ in [89] when comparing DP ViP model to non-DP SimCLR; or (3) rely on uncommon tricks such as a huge batch size from 16-98K, that are not adopted in the standard deep learning community. Related to (3), we believe DP continual pre-training can further improve using the existing techniques from the non-DP continual training, including the replay mechanism and curriculum learning, and avoid catastrophic forgetting.

Hessian-based analysis in deep learning Applying the second-order Taylor expansion of loss motivates the famous Newton’s method and is commonly adopted in deep learning [56, 93, 83, 55, 90], where the Hessian matrix is useful to analyzing the convergence and data efficiency (e.g. selecting the critical batch size [56]), even though it is infeasible to derive $\mathbf{H} \in \mathbb{R}^{d \times d}$ explicitly for large models. Our work follows the same path with a specific focus on DP related operations (i.e. the clipping and the noise). We use the Hutchinson method and Hessian-vector product to compute $\text{tr}(\mathbf{H})$, $\mathbf{H}\mathbf{G}$ and so on.

System design of DP training To make DP deep learning broadly applicable, we believe it is necessary to not only evaluate DP algorithms on the utility, but also from a system design perspective. The design of a DP system, such as our DP continual pre-training, should resemble that of the standard non-DP system (see our extensive discussion in Remark 4.3). Such a design will be compatible to and benefit from new advances in the much larger non-DP literature, unifying DP and non-DP communities, instead of crafting techniques that are limited to DP learning only.

Data distribution shift There may be some distribution shift between the *public* pre-training data and the *private* fine-tuning data or continual pre-training data. Empirically speaking, DP training can be robust to such distribution shift. For instance, DP fine-tuning has successfully transferred from ImageNet to CIFAR10, CIFAR100, SVHN, Food101, CelebA, FMNIST, GSTRB [11, 8], from JFT to ImageNet [23, 57], and from Places365 to ImageNet [46]. Although this work does not address the distribution shift due to similarity between ImageNet-1k and ImageNet-11k, our analysis in Section 3, especially the formula of decelerator, still holds in this scenario. Therefore, we expect our DP continual pre-training to work withstanding the data distribution shift, as empirically demonstrated from Shaders to LAION [89].

Concurrent work The concurrent work – ViP [89] – also studies the DP continual pre-training, thus is the closest strategy to ours. We elaborate the similarity and differences between two strategies.

Similarity

1. Both use ViT-Base as backbone and AdamW as optimizer.
2. Both use self-supervised learning (SSL) for public pre-training.
3. Both use $\epsilon = 8$ for DP continual pre-training.
4. Both public datasets (Shaders v.s. ImageNet-1k) have $\approx 1\text{M}$ images.

Differences

1. ViP uses SSL on DP continual pre-training. We use supervised learning.
2. ViP adds a decoder to ViT-Base (in total 99.0M parameters) during the pre-training. We replaces the classifier head of ViT-Base (94.4M parameters) for DP continual pre-training. Hence the model architecture is different.

3. ViP trains on Shaders (for 1.6B images) and LAION (for 0.6B images). We train on ImageNet-1k (for 0.3B images) and ImageNet-11k (for 0.4B images). Hence data distribution and quality is different, and our training requires about 1/3 the computation.
4. ViP’s private dataset (LAION) has 233M images. Ours (ImageNet-11k) has 12M images. Hence our training requires much smaller dataset (see Figure 3(a) [89]).
5. ViP has to use huge batch size 98K (see Figure 4(b) [89], where the loss diverges with batch size 8K). We use 4K.
6. ViP experiments with various model sizes, from ViT-Nano (18.6M) to Large (233M). We only use ViT-Base.